Check for updates

ADVANCED HEALTHCARE MATERIALS
www.advhealthmat.de

Bioprinting of Stem Cell Spheroids Followed by Post-Printing Chondrogenic Differentiation for Cartilage Tissue Engineering

*Monize Caiado Decarli, Adrián Seijas-Gamardo, Francis L. C. Morgan, Paul Wieringa, Matthew B. Baker, Jorge Vicente L. Silva, Ângela Maria Moraes, Lorenzo Moroni, and Carlos Mota**

Cartilage tissue presents low self-repair capability and lesions often undergo irreversible progression. Structures obtained by tissue engineering, such as those based in extrusion bioprinting of constructs loaded with stem cell spheroids may offer valuable alternatives for research and therapeutic purposes. Human mesenchymal stromal cell (hMSC) spheroids can be chondrogenically differentiated faster and more efficiently than single cells. This approach allows obtaining larger tissues in a rapid, controlled and reproducible way. However, it is challenging to control tissue architecture, construct stability, and cell viability during maturation. Herein, this work reports a reproducible bioprinting process followed by a successful post-bioprinting chondrogenic differentiation procedure using large quantities of hMSC spheroids encapsulated in a xanthan gum-alginate hydrogel. Multi-layered constructs are bioprinted, ionically crosslinked, and post chondrogenically differentiated for 28 days. The expression of glycosaminoglycan, collagen II and IV are observed. After 56 days in culture, the bioprinted constructs are still stable and show satisfactory cell metabolic activity with profuse extracellular matrix production. These results show a promising procedure to obtain 3D models for cartilage research and ultimately, an in vitro proof-of-concept of their potential use as stable chondral tissue implants.

1. Introduction

Osteoarthritis (OA) is one of the most frequent cartilage diseases reported, affecting ≈500 million people worldwide and being the leading cause of disability in elderly people.[1] Cartilage tissue presents low self-repair capability and the lesions often undergo irreversible progression toward diverse pathological conditions.[2] Non-surgical treatments for severe osteoarthritis are currently limited,[3] and with substantial less progress compared to therapies for other musculoskeletal diseases.[1] The only current cell-based approach approved by the FDA (in 2019) for cartilage repair is transplantation of autologous chondrocytes, and the treatment success depends on the severity of the case.[4] Despite being established for a long time, chondrocyte culture still presents limitations such as dedifferentiation when cultured for long periods or differentiation toward fibro or hypertrophic cartilage.[5–8]

Human mesenchymal stromal cells (hMSC) can be used to treat OA, but

M. C. Decarli, A. Seijas-Gamardo, F. L. C. Morgan, P. Wieringa, M. B. Baker, L. Moroni, C. Mota
MERLN Institute for Technology-Inspired Regenerative Medicine
Department of Complex Tissue Regeneration
Maastricht University
Universiteitssingel, 40, Maastricht, Limburg 6229 ER, the Netherlands
E-mail: c.mota@maastrichtuniversity.nl

The ORCID identification number(s) for the author(s) of this article can be found under https://doi.org/10.1002/adhm.202203021

© 2023 The Authors. Advanced Healthcare Materials published by Wiley-VCH GmbH. This is an open access article under the terms of the Creative Commons Attribution-NonCommercial-NoDerivs License, which permits use and distribution in any medium, provided the original work is properly cited, the use is non-commercial and no modifications or adaptations are made.

DOI: 10.1002/adhm.202203021

M. C. Decarli, Â. M. Moraes
Department of Engineering of Biomaterials and of Bioprocesses
School of Chemical Engineering
University of Campinas - UNICAMP
Av. Albert Einstein, 500, Cidade Universitária "Zeferino Vaz", Campinas, SP 13083-852, Brazil

J. V. L. Silva
Three-Dimensional Technologies Research Group
CTI Renato Archer
Rodovia Dom Pedro I SP-65, Km 143,6 - Amarais, Campinas, SP 13069-901, Brazil

21922659, 2023, 19, Downloaded from https://advanced.onlinelibrary.wiley.com/doi/10.1002/adhm.202203021 by Spanish Cochrane National Provision (Ministerio de Sanidad), Wiley Online Library on [26/01/2026]. See the Terms and Conditions (https://onlinelibrary.wiley.com/terms-and-conditions) on Wiley Online Library for rules of use; OA articles are governed by the applicable Creative Commons License

massive cell death is often observed after intra-articular injection. In OA rats, hMSC in 3D aggregates survived better than single cells, prolonging the survival of implanted tissues.[9] The differentiation of hMSC toward chondrogenic lineage is highly efficient in aggregates and has been established since the 1960s.[5] Also, when cultured in 3D, the dedifferentiated phenotype commonly observed in late 2D subcultures can be reversed to normal chondrocyte phenotype as a result of the improved cell-to-cell contact.[4,6]

Several approaches have been investigated over the last decades to generate cartilage tissue engineered constructs. Extrusion bioprinting processes comprising spheroid-loaded bioinks is one of these, and it was first reported by Mironov et al.[10] and Jakab et al.[11]. Due to cell aggregation followed by extracellular matrix (ECM) production typically observed in spheroids, these bioprinted constructs start in a more advanced stage of maturation and faster tissue formation is expected when compared to bioprinting of single cells.[12,13]

Bioprinting processes with spheroid-loaded bioinks enable the use of a much higher concentration of cells,[14] overcoming cell density limitation of conventional bioprinting approaches.[15] Cells pre-arranged in uniform and spherical aggregates can be placed in specific positions using a controlled and reproducible technique. This allows the modulation of contact and fusion with neighboring spheroids to obtain larger, mechanically stable tissues.[14] Thus, this process can offer substantial gains in terms of flexibility, productivity, and scalability.[16]

Extrusion bioprinting processes comprising spheroid-loaded bioinks is still challenging as several consideration needs to be taken into account. First, a nozzle with a diameter considerably bigger than the spheroid size is required, to ensure low shear-stress and to avoid cell damage.[17] Due to molecular diffusional limitations, the maximum diameter of a spheroid in which no necrotic core is observed ranges from 100–200 µm, depending on the cell type.[17] For cartilage tissue, spheroid diameter values of ≈480 µm using cartilage progenitor cells with 88% of cell viability were already reported, however these were not bioprinted.[18] Thus, since the printing resolution is mainly limited by the dispensing nozzle diameter,[15] the spatial resolution of the final construct may be limited if large spheroids are used.[19] Therefore, achieving pattern fidelity and high resolution similar to bioprinting single cells is still a challenge.

During the bioprinting process, it is also essential to provide an appropriate microenvironment that can keep spheroids in suspension, acting as an ECM-like material for cell proliferation and differentiation.[20,21] The use of hydrogels is a successful strategy due to their hydrated nature that resembles the native ECM microenvironment[21] while serving as support material[22] allowing also cell sprouting and migration.[23] As reviewed by Mota et al.,[24] despite several hydrogels having been formulated for bioprinting, it is still challenging to obtain a cell-relevant material capable of mimicking the tissue environment and simultaneously allowing efficient bioprinting.

For cartilage tissue engineering, hydrogels consisting of natural polymers are attractive with regard sustaining round-shaped chondrocytes.[25] Alginate (A) is an example of such polymers and it is one of the most frequently investigated classes of bioink components.[24] Alginate is a biocompatible unbranched polysaccharide composed of mannuronic (M) and guluronic (G) acids that can be efficiently crosslinked by divalent ions, with Ca^{2+} being the most extensively used for viable cell encapsulation.[26] Also, characteristics such as solubility, degradability, and shear-thinning properties are major advantages that can be tuned by the Ca^{2+} induced gelation. Alginate is also frequently combined with other compounds (e.g., fibrinogen, chitosan, collagen, arginine-glycine-aspartate, or heparin-binding peptides and even with decellularized ECM components) to fabricate ECM-mimicking scaffolds to improve both cell attachment and mechanical properties of a bioink.[27–30]

An interesting polysaccharide not yet frequently explored as a component of bioink formulations is xanthan gum (XG). XG is a branched-chain polysaccharide commercially produced by the bacterium *Xanthomonas campestris* and widely used in the food and pharmaceutical industries due to its characteristics of non-toxicity, high viscosity at low concentrations, emulsion-stabilizing activity, and pseudoplastic rheological properties.[31] XG is also very stable at different conditions of pH, temperature, and ionic concentrations,[32] as well as showing shear-thinning properties.[33] XG is particularly interesting due to its capability to protect the articular cartilage. Previous reports show that intra-articular XG injections alleviate the effects of cartilage degradation, with significant improvement of fissures, loss of chondrocytes, along with increment of cartilage matrix, reducing the damage in osteoarthritis in animal models.[34,35] XG has been recently blended with other polymers to achieve optimal mechanical properties, such as gellan gum[36] and a carboxymethyl chitosan/methylcellulose combination for bone and cartilage applications, respectively.[37]

Recently, several reports have showed that cartilage constructs could be successfully bioprinted with pre-differentiated spheroids. For this, stem cells spheroids are frequently cultured in different chondrogenic growth factors and harvested at different chondrogenic maturation stages, generally at day 7, 14, 21, or 28 of differentiation in vitro. These chondrogenic induced spheroids are subsequently bioprinted to achieve a cartilage-like construct.[38–42] On the other hand, Hall et al.[43] reported that spreading, fusion and remodeling capacities of cartilaginous spheroids decreased with prolonged differentiation periods in vitro. To overcome this limitation, we introduced herein a novel post-bioprinting differentiation method, while aiming to maintain fusion and remodeling capacities of stem cell spheroids. Our approach could boost the generation of mature tissue as well as offer a first in vitro proof-of-concept for in situ chondrogenic differentiation post-implantation. Therefore, eventually reducing the needed time to develop patients-specific chondrogenic implants and increasing the chances in terms of flexibility and scalability, when compared with bioprinting approaches involving pre-differentiated spheroids.

The aim of this study was to generate stem cell constructs that could be differentiated toward cartilage in a post-bioprinting approach. Two natural polysaccharides (alginate and XG) combined with hMSCs spheroids were investigated to formulate bioinks and to produce stable bioprinted constructs. Rheological analysis was performed for four different hydrogel formulations. A pressure-assisted extrusion bioprinting process was used and a set of parameters was investigated to ensure suitable construct resolution. HMSC spheroids were encapsulated in the alginate-XG hydrogel and the bioprinted constructs were produced and

© 2023 The Authors. Advanced Healthcare Materials published by Wiley-VCH GmbH

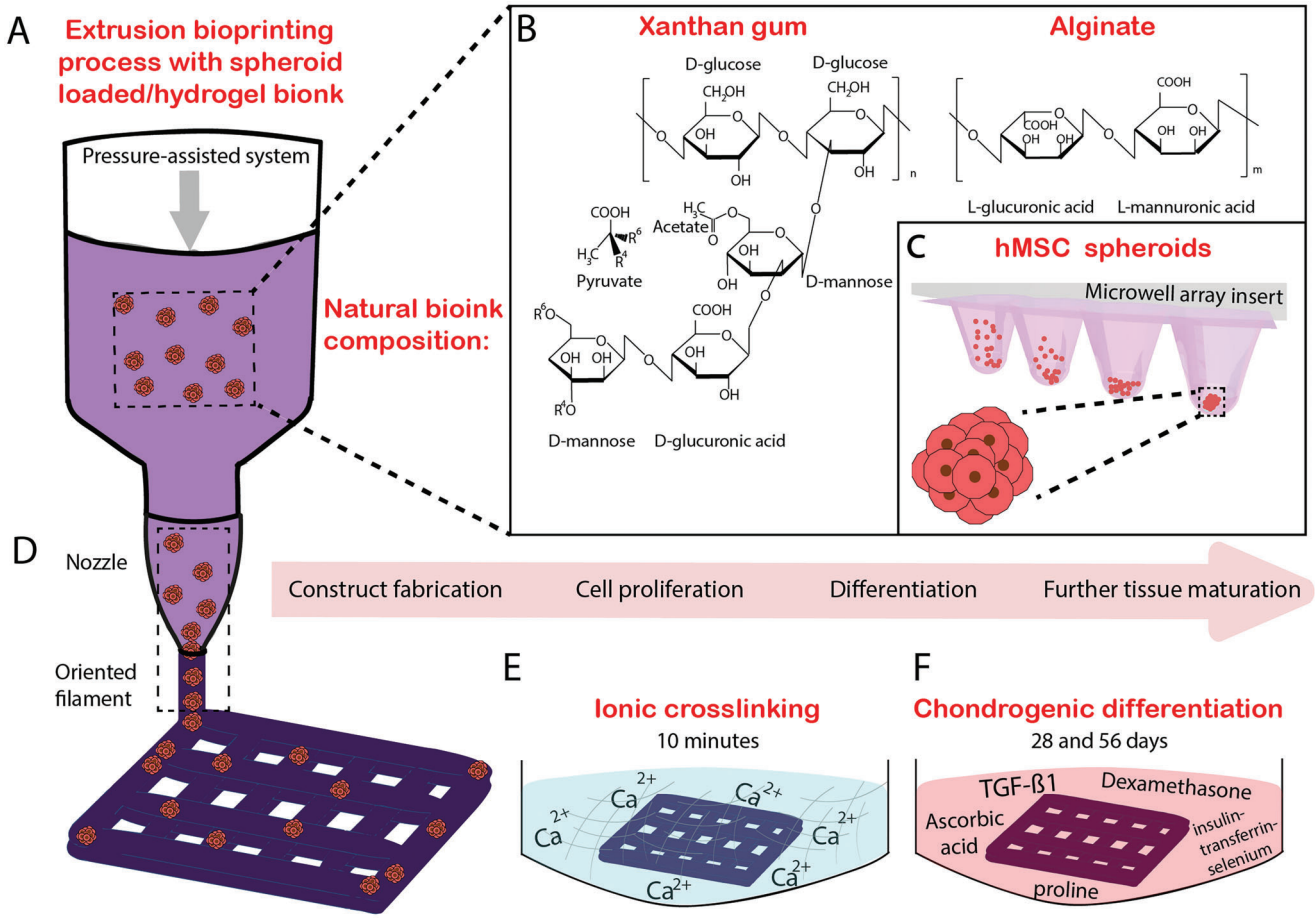

Figure 1. Schematic illustration of the bioprinting process with spheroid-loaded/hydrogel-bioinks developed in this work. A) Bioprinting method to form 3D constructs by the deposition of cell spheroids, suspended in a homogeneous printable hydrogel. B) The bioink was composed of mixtures of xanthan gum and alginate, capable to crosslink with Ca^{2+} ions. C) HMSC spheroids were obtained by culturing cells in a 3D microenvironment in non-cell-adhesive agarose hydrogel array inserts. D) By applying controlled pressure, the bioink was extruded through the nozzle in the form of a filament on pre-designed patterns to manufacture the constructs. E) Constructs with proliferating cells were ionically crosslinked using calcium chloride and, subsequently, F) differentiated using chondrogenic medium over 28 and 56 days to obtain chondral constructs.

ionically crosslinked. A post-printing differentiation procedure towards cartilage was performed on spheroid-loaded constructs for 28 days and their stability was analyzed for supporting both spheroid differentiation and maturation processes. In general, this approach provided fundamental insights into the bioprinting process using 3D cell spheroids as a promising procedure to obtain stable chondrogenic constructs. A schematic illustration of the steps performed in this study is presented in **Figure 1**.

2. Results

2.1. Development of Xanthan Gum-Alginate Hydrogels

The appropriate biomaterial formulation to combine with spheroids was first optimized aiming at using extrusion bioprinting. The biomaterial formulation needs to have shear thinning properties and retain its shape upon extrusion. It should also undergo crosslinking to enable long-term stability (at least 28 days) in culture medium, while keeping spheroids viable and able to differentiate. With these criteria in mind, along with the attractive characteristics of both natural polysaccharides above-mentioned, multiple combinations of XG and A were tested.

Prior to test the combinations of XG and A, the sterilization process and crosslinking mechanism of XG was investigated. Due to the high viscosity, XG could not be filtered (Figure S1A, Supporting Information) and autoclaving (121 °C, 20 min cycle) resulted in some level of degradation (Figure S1B, Supporting Information). Hence, sterilization by autoclaving of the polysaccharide powder (pre-vacuum, 134 °C, 4 min cycle) was the most feasible approach. Since no mild and biocompatible crosslinking mechanism is available for XG without requiring further chemical modification of the polysaccharide, A was added to all formulations for its well-known ability to form stable ionic crosslinks in the presence of bivalent ions such as Ca^{2+}. As expected, scaffolds consisting solely of XG were completely dissolved after 48 h, even when exposed to $CaCl_2$ solution (125 mM, 10 min) (Figure S2, Supporting Information). The vial inversion test (Figure S3, Supporting Information) revealed that only formulations containing A, with a total polysaccharide concentration above 4.75% (*w*/*v*) and at least twice as much XG as A were able to resist flowing

© 2023 The Authors. Advanced Healthcare Materials published by Wiley-VCH GmbH

21922659, 2023, 19, Downloaded from https://advanced.onlinelibrary.wiley.com/doi/10.1002/adhm.202203021 by Spanish Cochrane National Provision (Ministerio de Sanidad), Wiley Online Library on [26/01/2026]. See the Terms and Conditions (https://onlinelibrary.wiley.com/terms-and-conditions) on Wiley Online Library for rules of use; OA articles are governed by the applicable Creative Commons License

21922659, 2023, 19, Downloaded from https://advanced.onlinelibrary.wiley.com/doi/10.1002/adhm.202203021 by Spanish Cochrane National Provision (Ministerio de Sanidad), Wiley Online Library on [26/01/2026]. See the Terms and Conditions (https://onlinelibrary.wiley.com/terms-and-conditions) on Wiley Online Library for rules of use; OA articles are governed by the applicable Creative Commons License

over 24 h. This is not surprising, as higher proportions of the low viscosity alginate solution would reduce the overall viscosity of the formulations. The four formulations that were observed to be more stable were selected for further characterization studies.

2.2. Characterization of Xanthan Gum-Alginate Hydrogels

The four stable precursor hydrogels were bioprinted after empirical optimization of the process parameters (**Figure 2**A). It was observed that printability, as indicated by the pore size and the number of visible pores, increased as the XG ratio increased. Indeed, a control print of the hydrogel consisting solely of XG without A showed an even better printability (Figure 2A). These results indicate that the printability of the precursor hydrogel is primarily dictated by the total XG content.

The efficacy of printing the stable precursor hydrogels directly into a bath of calcium chloride crosslinking solution was also analyzed, but since the printed filaments could not attach to the well plate, this strategy was not further used (Figure S4, Supporting Information). To decide which of the stable precursor hydrogels to select for further studies, the shear moduli pre- and post-crosslinking (Figure 2B), strain response (Figure 2C) and flow behavior (Figure 2D) were analyzed by rheometry. The shear modulus of the non-crosslinked hydrogels increased from 230 to 410 Pa as the XG content increased from 3.33% to 4.1% (*w/v*), showing the same trend with respect to printability, as higher viscosity led to less filament coalescence. Similarly, the shear modulus of the crosslinked hydrogels increased from 590 to 2210 Pa as the proportion of alginate increased from 0.75% to 1.5% (*w/v*). This trend was also expected, as more alginate allows for more crosslinking points to be formed, increasing both network density and shear modulus.

Strain sweeps of the non-crosslinked hydrogels showed no significant difference in the linear viscoelastic region, with all formulations exhibiting strain-independent behavior up to 10% strain. Time and frequency sweeps were also performed (Figure S5, Supporting Information), showing stable shear moduli immediately after loading, and negligible frequency dependence in the plateau region of the frequency response spectrum. Interestingly, the flow curves of each non-crosslinked formulation showed very little difference, with a slight yield point observable at a strain rate of 10^{-1} s^{-1}, and a near-uniform flow profile following this threshold. The observed yielding behavior occurred at strain rates significantly below those applied during extrusion. The observed flow behavior would suggest that the difference in printability is derived mainly from material viscosity, where higher values limit flow (deformation) post-extrusion. To explore this further, a time sweep was performed immediately following the flow curve (Figure S5, Supporting Information). These time sweeps showed that above 50% of the initial shear modulus was recovered before the first measured data point across all formulations. Consequently, formulations with high initial moduli (and viscosities) lead to higher viscosities immediately following extrusion, and thus reduced flow and higher printing fidelity.

2.3. Effects of Printing Conditions on Scaffold Characteristics

In the absence of significant differences in flow behavior, the $XG_{3.75}$:$A_{1.12}$ formulation was chosen for further studies, since it presented the highest amount of A, ensuring feasible amount of visible macropores. Furthermore, the higher amount of A ensured an overall construct stability for the envisioned culture duration. Long culture periods are important due to the maturation process, in which the construct should show stability enough to support cell proliferation, differentiation and the production of ECM molecules.

Printing with the $XG_{3.75}$:$A_{1.12}$ formulation by varying both pressure and deposition speed was evaluated regarding structural stability to enable long culture period. Considering printability, a range of optimal printing parameters was considered, including printing speed from 40 to 60 mm s^{-1} and extrusion pressure from 50 to 70 kPa. However, constructs bioprinted at 40 mm s^{-1} and 50 kPa or 60 kPa were less stable, losing their conformation at day 50 (Figure S6, Supporting Information). The remaining printing conditions led to high scaffold stability for 50 days.

With these optimized conditions, regular and well-defined filaments of $XG_{3.75}$:$A_{1.12}$ hydrogels were obtained (Figure 2E). The filament diameter was modulated by changing the nozzle gauge with internal diameters from 250 to 410 μm. In both cases, the filaments obtained had bigger diameters when compared to the nozzle internal diameter, with an increase of 57% (394 ± 55 μm) and 45% (598 ± 74 μm) for 250 and 410 μm, respectively (Figure 2E). This phenomenon was expected due to the coalescence of the hydrogel in some parts of the structure after the extrusion process and was taken into account when bioprinting multilayered structures.

Constructs were obtained with porosity and printing fidelity higher than those attained with any of the formulations previously investigated (Figure 2F), with well-defined pores (Figure S7A, Supporting Information). The pore size presented an average of 38 ± 10 μm in *X*-axis and 51 ± 14 μm in *Y*-axis, representing a total construct porosity of 58 ± 17% of that predicted in the original CAD design (Figure 2F). As a proof of concept for future studies, 10-layer scaffolds were bioprinted, which were capable of maintaining their structure stability during handling and showed a constant morphology throughout the height (Figure S7B, Supporting Information).

Finally, to verify if the chosen material was capable of supporting cell culture for at least the time necessary to perform the differentiation process (minimum of 28 days), the swelling and mass loss was analyzed by immersing the hydrogel in culture media (Figure 2G). An increasing linear trend in swelling was observed, and the biological constructs reached a final swelling ratio of 147 ± 28% after 28 days. Interestingly, scaffold degradation and mass loss over the 28 days of culture were expected, since the polysaccharides could revert back to solution due to ion exchange between calcium and other monovalent ions present in the medium culture. Instead, a mass gain was observed over this period, possibly resulting from increased retention of culture medium components.

2.4. Characterization of 5 and 7-day hMSC Spheroids to be Used as Bioink Cellular Components

HMSC spheroids cultured for 5 and 7 days in basic media were investigated to be used as cellular components of the spheroid-loaded bioink and no significant difference in terms of

© 2023 The Authors. Advanced Healthcare Materials published by Wiley-VCH GmbH

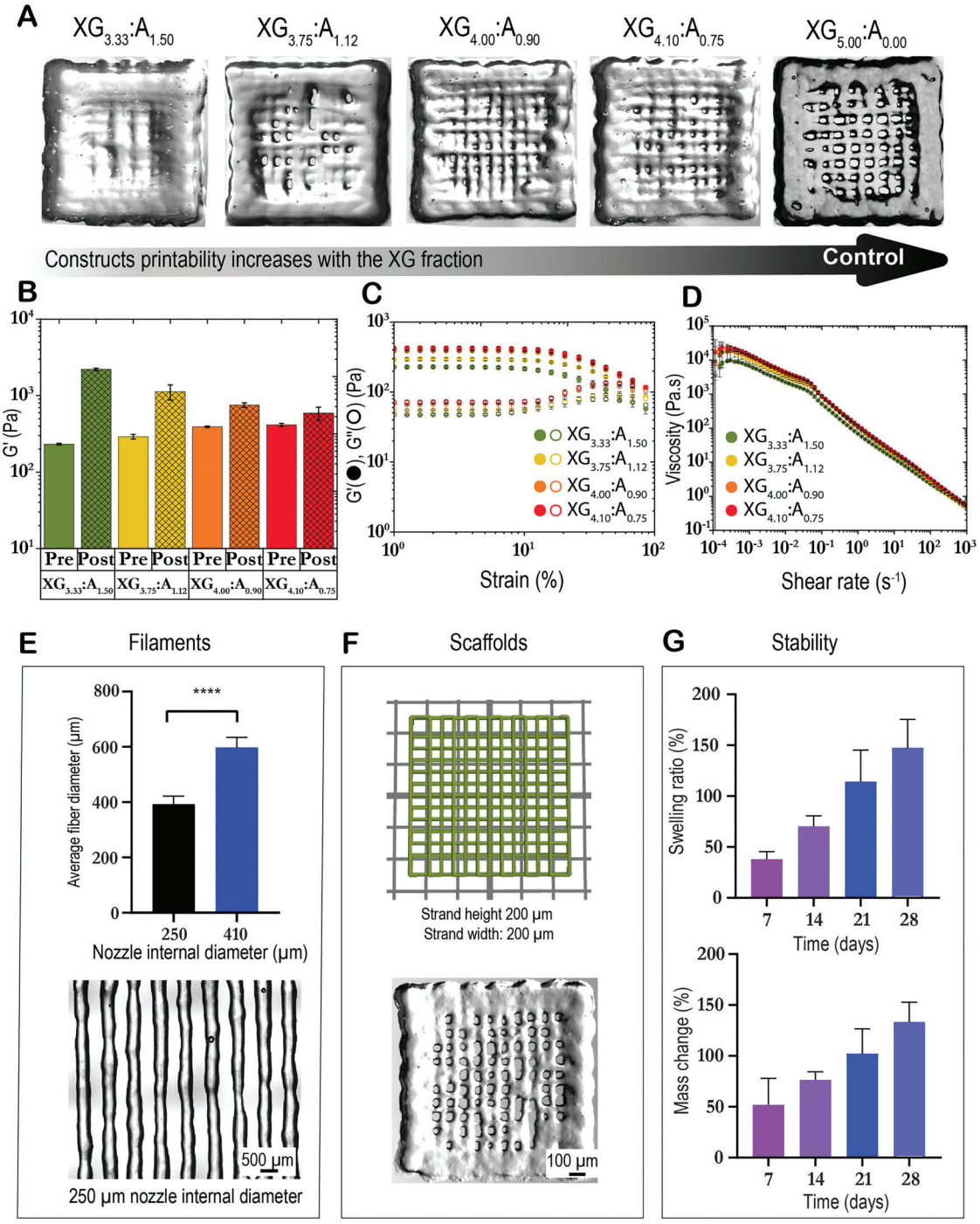

Figure 2. Development and characterization of a natural polysaccharide hydrogel made of alginate (A) and xanthan gum (XG): A) constructs printability increases with XG fraction, indicated by pore size and number of visible pores of a 4-layer structure using the four stable precursor hydrogels. Rheological characterization of stable XG:A formulations based on B) shear moduli (pre- and post-crosslinking); C) strain response and D) flow behavior considering storage modulus (G′) and loss modulus (G″). The post-crosslinking samples were treated with $CaCl_2$ (125 mM, 10 min) to crosslink alginate molecules. Characterization of $XG_{3.75}$:$A_{1.12}$ printed hydrogels: E) regular filaments of ≈400 and 600 μm in diameter can be obtained by changing the nozzle size (13 filaments of three independent scaffolds were quantified). Well-defined filaments were obtained using the nozzle with 250 μm internal diameter. F) Scaffolds with adequate porosity can be obtained (scale bar 100 μm), following the predicted original CAD design (green). G) Progressive increase in both scaffold swelling ratio and mass gain over 28 days in culture medium. In all experiments, the printed scaffolds were analyzed in at least triplicate.

© 2023 The Authors. Advanced Healthcare Materials published by Wiley-VCH GmbH

21922659, 2023, 19, Downloaded from https://advanced.onlinelibrary.wiley.com/doi/10.1002/adhm.202203021 by Spanish Cochrane National Provision (Ministerio de Sanidad), Wiley Online Library on [26/01/2026]. See the Terms and Conditions (https://onlinelibrary.wiley.com/terms-and-conditions) on Wiley Online Library for rules of use; OA articles are governed by the applicable Creative Commons License

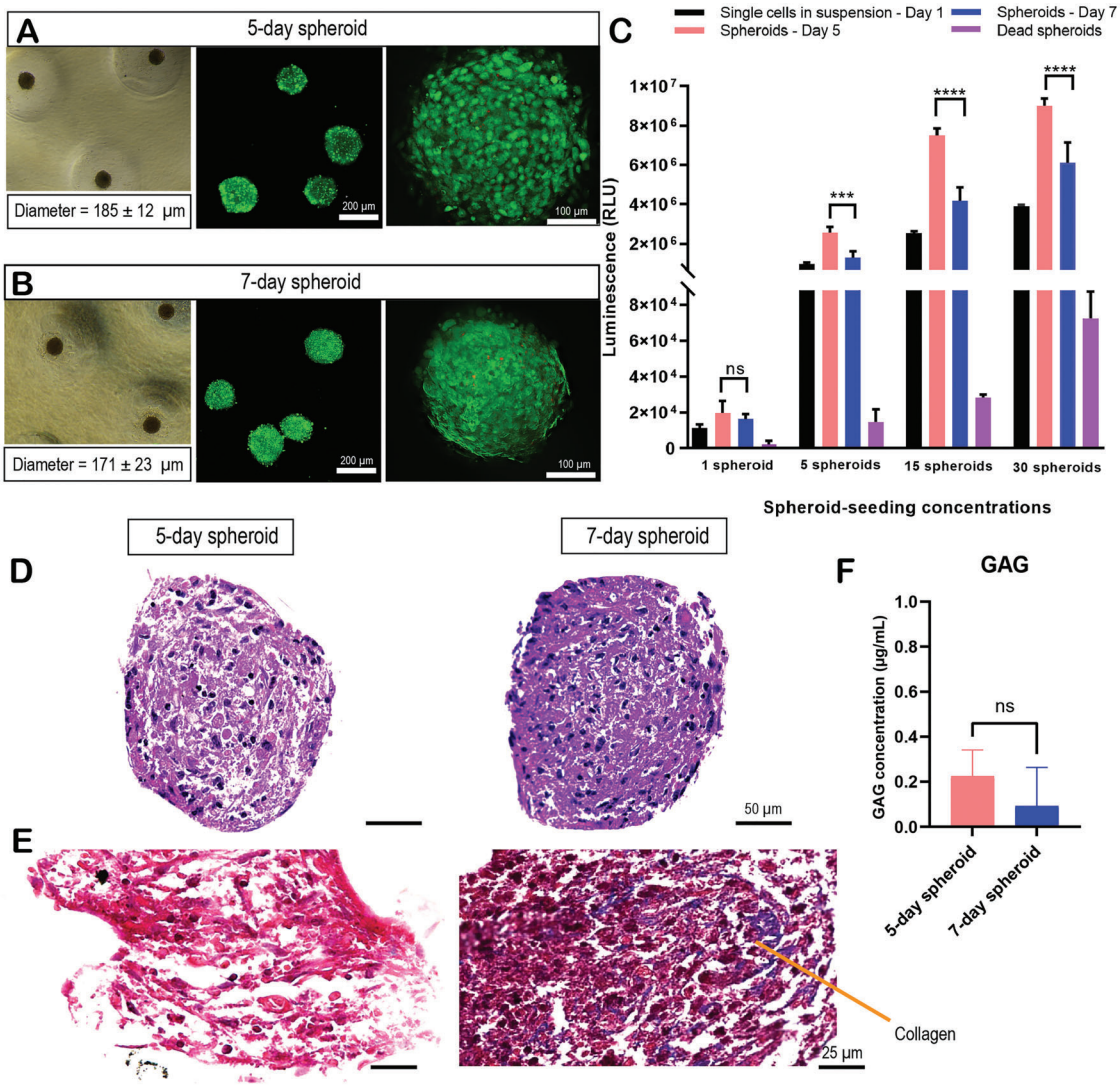

Figure 3. Comparative analysis between 5 and 7-day hMSC spheroids to be used as bioink cellular components: A) Morphological comparison of 5 day spheroids produced using the microwell array insert, staining of live cells (calcein AM, green) and non-viable (EthD-1, red) and average diameter (15 spheroids were evaluated) of spheroids harvested from the device. B) Same comparison for 7-day spheroids. C) Metabolic activity of single cells immediately before the aggregation, and of 5 and 7-day spheroids at four concentrations (1, 5, 15, and 30 spheroids); significant differences (***, $p \leq 0.001$, **** $p \leq 0.0001$) and non-significant (ns), as determined by the Tukey's multiple comparison test. DMSO-treated spheroids were used as non-viable controls to evaluate the ATP readout levels. The results showed that the ATP levels measure for these non-viable spheroids was drastically reduced. D) Representative images of cell nuclei and cytoplasm organization (HE staining, performed in triplicate) of 5 and 7-day hMSC spheroids. E) Absence and presence of collagen (MT staining, performed in triplicate) in 5 and 7-day spheroids. F) GAG quantification of 5 and 7-day spheroids maintained in basic culture media.

morphology and cell viability were observed (**Figure 3**A,B). The average diameters of the spheroids were 185 ± 12 and 171 ± 23 µm for days 5 and 7, respectively. Both types of spheroids exhibited similar regular spherical shape and 7-day spheroids were more compact than 5-day. High cell viability in both groups was observed (Figure 3A,B). On the other hand, differences were detected when comparing the metabolic activity of the cells at concentrations equivalent to those of 5 and 7 days-old spheroids (Figure 3C). For the four spheroid seeding concentrations tested, higher metabolic activity was noticed in 5-day spheroids, which released high levels of ATP. Conversely, as the spheroid formation time increased from 5 to 7 days, the metabolic activity decreased in all four spheroid tested groups, emphasizing that 5-day spheroids seem to be the most promising for bioprinting.

Histological analysis using hematoxylin-eosin stain showed a comparable distribution of cell nuclei (dark blue) and cytoplasm (pink) in 5 and 7-day spheroids (Figure 3D). Collagen fibers analyzed using Masson's trichrome stain were not detected in 5-day spheroids (Figure 3E), but the presence of clusters of collagen fibers (blue) is evident in the 7-day cell aggregates. There is no GAG deposition in 5- and 7-day spheroids cultured in basic media, since the levels were statistically similar and near to zero on the calibration curve (Figure 3F). Since the spheroid maturation process would continue for long periods once the constructs are

© 2023 The Authors. Advanced Healthcare Materials published by Wiley-VCH GmbH

21922659, 2023, 19, Downloaded from https://advanced.onlinelibrary.wiley.com/doi/10.1002/adhm.202203021 by Spanish Cochrane National Provision (Ministerio de Sanidad), Wiley Online Library on [26/01/2026]. See the Terms and Conditions (https://onlinelibrary.wiley.com/terms-and-conditions) on Wiley Online Library for rules of use; OA articles are governed by the applicable Creative Commons License

21922659, 2023, 19, Downloaded from https://advanced.onlinelibrary.wiley.com/doi/10.1002/adhm.202203021 by Spanish Cochrane National Provision (Ministerio de Sanidad), Wiley Online Library on [26/01/2026]. See the Terms and Conditions (https://onlinelibrary.wiley.com/terms-and-conditions) on Wiley Online Library for rules of use; OA articles are governed by the applicable Creative Commons License

bioprinted, 5-day spheroids were used for bioprinting studies, as they are composed of more metabolically active cells.

Once defined hMSC 5-day spheroids for bioprinting studies, time lapses microscopies were performed to prove their capacity to completely fuse into a round sphere when closely placed and encapsulated in the XG/A hydrogel. As can be clearly seen (Figure S8, Supporting Information), after 20 h, an ellipsoid (length *y*-axis = 291 μm/length *x*-axis = 449 μm) was formed by the fusion of two spheroids. Finally, after 46 h and complete remodeling of its internal structure, a spheroid was formed (length *y*-axis = 360 μm/length *x*-axis = 322 μm). Thus, we introduced herein a novel post-bioprinting differentiation method that can maintain the fusion and remodeling capacities of stem cell spheroids.

Finally, aiming to analyze the sensitivity of hMSC spheroids to shear forces of different intensities, a live/dead assay was performed before and after gentle or vigorous pipetting steps (Figure S9, Supporting Information). High cell viability could be detected using gentle pipetting compared to a substantial increase in the number of dead cells detected when vigorous pipetting was applied. Dead cells were observed on the outermost surface of some spheroids (yellow arrows), along with nonviable spheroids (blue arrows). Because of this, two mixing approaches involving gentle and vigorous shear forces (Figure S10, Supporting Information) were evaluated to guarantee a uniform distribution of spheroids, while ensuring high cell viability. The reduced shear stress strategy (gentle mixing) of spheroids into the hydrogel was more effective at protecting the spheroid surfaces when compared to vigorous mixing. Furthermore, it represented a simple manner to obtain a more homogeneous distribution of spheroids in the bioprinter's cartridge. Indeed, the filaments of the final construct presented a more uniform distribution of spheroids when compared to that achieved with vigorous mixing (Table S4, Supporting Information).

2.5. Bioprinting of Spheroid-Loaded Constructs and Cell Viability for 28 Days

Stable bioprinted constructs containing 5-day spheroids were obtained. Four-layered 1 × 1 cm constructs presented average weight of 5.2 ± 0.4 mg and thickness of ≈2 mm (**Figure 4**A). The 3D spherical structure and uniform shape of the spheroids were preserved 7 days after bioprinting (Figure 4B) and bioprinted hydrogel filaments measuring 396 ± 43 μm were capable to maintain the spheroids (153 ± 22 μm) in a stable manner (Figure 4C). From the first day onward, detachment of cell clusters from the spheroids could be observed (Figure 4D). Despite the spheroids were dispersed throughout the 1 × 1 cm scaffold during bioprinting in a satisfactory way, they tended to be more concentrated on the external borders of the filaments, where extra material deposition occurred, increasing filament coalescence. Furthermore, the open-pore structure was gradually lost as the number of bioprinted spheroids per construct increased (Figure 4E).

High cell viability was observed for fully encapsulated spheroids in bioprinted constructs throughout the 28 days in culture (Figure 4F). On day 14, confocal microcopy evaluation was performed to analyze in detail the innermost parts of the spheroids, aiming to investigate the presence of necrotic cores as the result of hypoxia and insufficient nutrients. The presence of a considerable population of live cells (green) along with a small percentage of dead cells (red) and absence of necrotic cores was confirmed.

To investigate if the bioprinted spheroids could maintain the metabolic activity after the bioprinting process, ATP measurements were performed (Figure 4G). The metabolic activity of the spheroids increased by 58% at day 2 and 43% at day 7 when compared to the ATP values obtained immediately after bioprinting (day 0). Thus, the bioprinting process did not significantly affect the cells. Only at day 14 a reduction to 76% of metabolic activity could be observed, which was maintained at values statistically similar at day 21 (51%) and day 28 (55%).Thus, culturing fully encapsulated hMSC spheroids in basic medium after the bioprinting process resulted in overall satisfactory cell viability.

The morphology of the spheroids was maintained during 28 days after bioprinting, with no significant variation (Figure 4H). Average spheroid diameters reduced from 185 ± 12 μm (in *X* axis) and 183 ± 12 μm (in *Y* axis) before bioprinting to 140 ± 21 μm (in *X* axis, 24% size reduction) and 141 ± 20 μm (in *Y* axis, 23% size reduction) 28 days after bioprinting. The analysis of the sphericity index showed a variation of 0.90 ± 0.1 before printing to 0.95 ± 0.01 at day 28 and confirmed that spheroids retained their highly regular spherical shape over time.

2.6. Post-Printing Chondrogenic Differentiation to Obtain Chondral Constructs

The potential for hMSCs' chondrogenic differentiation was initially confirmed using the cell pellets standard protocol (Figure S11A,B, Supporting Information). The bioprinted constructs subjected to chondrogenic differentiation were analyzed for morphology and cell migration. First, spheroids maintained their regular and spherical shape (**Figure 5**A). As previously observed for basic medium (Figure 4D), some cells also detached from the spheroid toward the hydrogel when chondrogenic medium was used, but this phenomenon was much more pronounced and a complete rearrangement on the outer layer in most of spheroids could be observed at day 28 (Figure 5B). This rearrangement was not only driven by the ECM expansion, but also resulted from cell migration, as observed in some spheroids by cell nuclei immunostaining (blue). The same phenomenon was not observed when the spheroids were cultured in basic medium for 28 days with effective preservation of the high sphericity and solidity indexes, as previously presented (Figures 4F,H). Due to this noticeable ECM expansion, spheroids cultured in chondrogenic and basic media for 28 days were measured (Figure 5C). The chondrogenic culture resulted in spheroids with 82 ± 30 μm, being two times bigger in diameter compared with spheroids maintained in basic culture media (39 ± 8 μm). The metabolic activity of bioprinted hMSC spheroids at day 28 cultured in basic or chondrogenic culture media was also compared and the cell metabolic activity was significantly higher in chondrogenic medium (Figure 5D).

GAG deposition was clearly observed in the bioprinted constructs subjected to chondrogenic differentiation for 28 days (Figure 5F) in contrast to its absence in constructs cultured in basic medium for 28 days (Figure S11C, Supporting Information) and in constructs at day 1, before starting the differentiation

© 2023 The Authors. Advanced Healthcare Materials published by Wiley-VCH GmbH

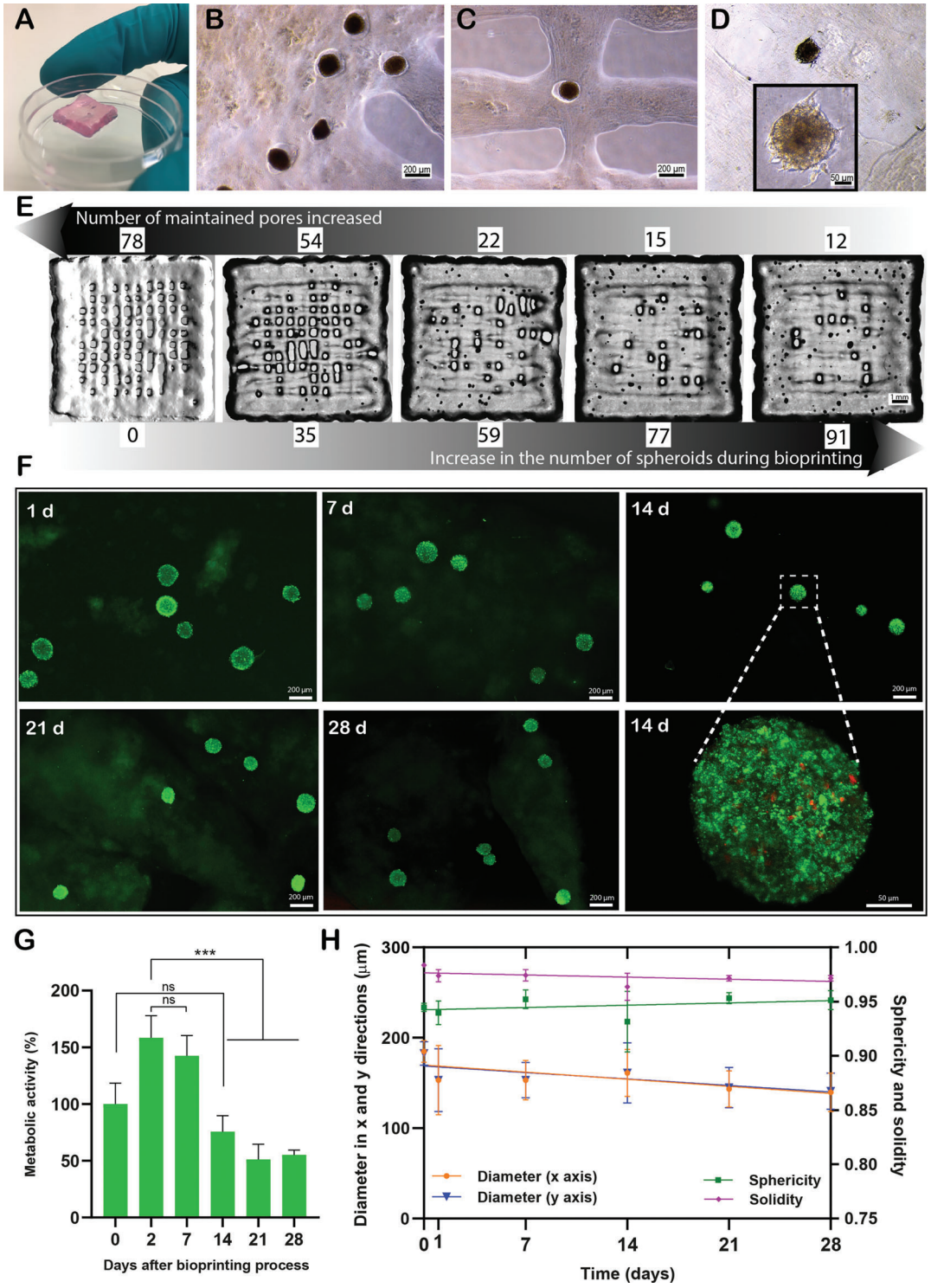

Figure 4. Extrusion bioprinting process with the spheroid-loaded bioink. A) Typical visual aspect of 4-layered bioprinted constructs made of hMSC spheroids and $XG_{3.75}$:$A_{1.12}$ hydrogel. B) Spheroids maintained their 3D conformational structure 7 days after bioprinting. C) Size proportion between printed filaments and hMSC spheroid incorporated in the hydrogel 7 days after bioprinting. D) Detachment of some cells from the 3D spheroid structure toward the hydrogel. E) In a clear trend, the open-pore structure was gradually reduced as the number of printed spheroids per construct increased. F) Live/dead staining (live cells in green, calcein AM and dead cells in red, EthD-1) of hMSC spheroids incorporated in the $XG_{3.75}$:$A_{1.12}$ hydrogel over 28 days and a detailed analysis on day 14 through by confocal microscopy. G) Metabolic activity of hMSC cells organized in spheroids incorporated in $XG_{3.75}$:$A_{1.12}$ hydrogel over 28 days after bioprinting. Two independent experiments were performed with 10 spheroids at each time point in triplicate samples; significant differences ***, $p \leq 0.001$, and non-significant, ns, were determined by the Tukey's multiple comparisons test. H) No differences were noticed in spheroids morphology over 28 days after printing when compared to day 0. All studies were performed using basic medium.

© 2023 The Authors. Advanced Healthcare Materials published by Wiley-VCH GmbH

21922659, 2023, 19, Downloaded from https://advanced.onlinelibrary.wiley.com/doi/10.1002/adhm.202203021 by Spanish Cochrane National Provision (Ministerio de Sanidad), Wiley Online Library on [26/01/2026]. See the Terms and Conditions (https://onlinelibrary.wiley.com/terms-and-conditions) on Wiley Online Library for rules of use; OA articles are governed by the applicable Creative Commons License

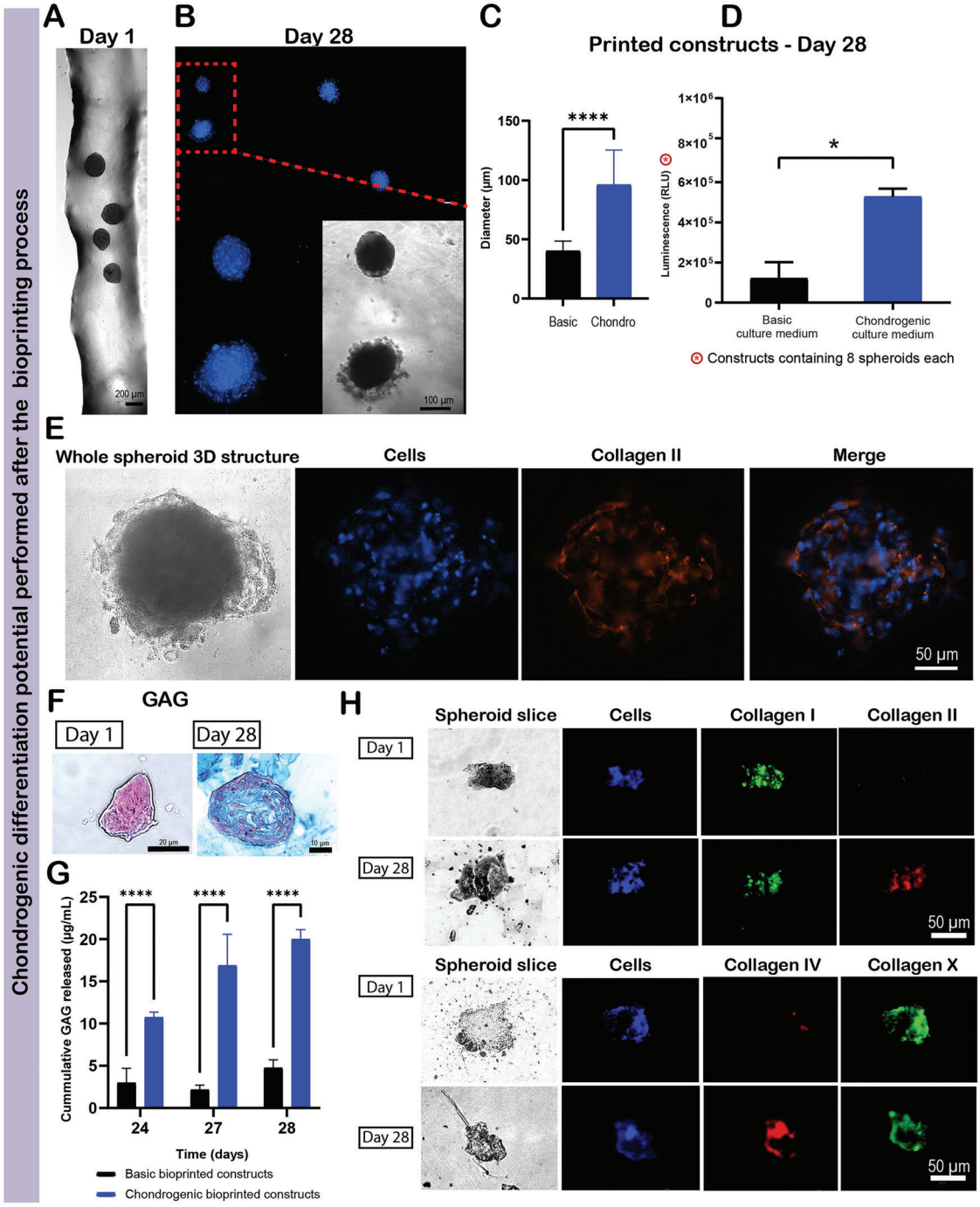

Figure 5. Post-printing chondrogenic differentiation of hMSC spheroids incorporated in $XG_{3.75}$:$A_{1.12}$ hydrogel over 28 days after bioprinting. A) Representative images of the regular and the spherical surface of spheroids one day after bioprinting, to compare with the B) rearrangement of ECM and cell migration from the outer layer of the spheroids toward the hydrogel, after cultured in chondrogenic media for 28 days. C) Diameter of spheroids cultured in basic and chondrogenic media for 28 days (13 spheroids of two independent bioprinting experiments). D) Comparative analysis of the cell metabolic activity between printed constructs cultured in basic or chondrogenic culture media for 28 days, in which two independent bioprinting experiments were performed with 8 spheroids on each construct in triplicate samples (significant differences *, $p \leq 0.05$, was determined by the unpaired two-tailed *t*-test). E) Chondrogenic differentiation potential performed after the bioprinting process was confirmed by the presence of collagen II (red, by immunostaining) performed in the whole spheroid structure and F) GAG deposition after culture in chondrogenic media for 28 days (blue, GAG, alcian blue staining) comparable with no deposition at day 1, before starting the differentiation process (pink, cells, alcian blue staining, performed in spheroid slices). G) Quantification of cumulative GAG release in chondrogenic and basic bioprinted constructs. H) Investigation of the presence of collagens I, II, IV, and X at day 1 and 28 days after the bioprinting and differentiation processes performed in spheroid slices. All staining procedures were performed in triplicate. All studies were performed using chondrogenic medium.

© 2023 The Authors. Advanced Healthcare Materials published by Wiley-VCH GmbH

21922659, 2023, 19, Downloaded from https://advanced.onlinelibrary.wiley.com/doi/10.1002/adhm.202203021 by Spanish Cochrane National Provision (Ministerio de Sanidad), Wiley Online Library on [26/01/2026]. See the Terms and Conditions (https://onlinelibrary.wiley.com/terms-and-conditions) on Wiley Online Library for rules of use; OA articles are governed by the applicable Creative Commons License

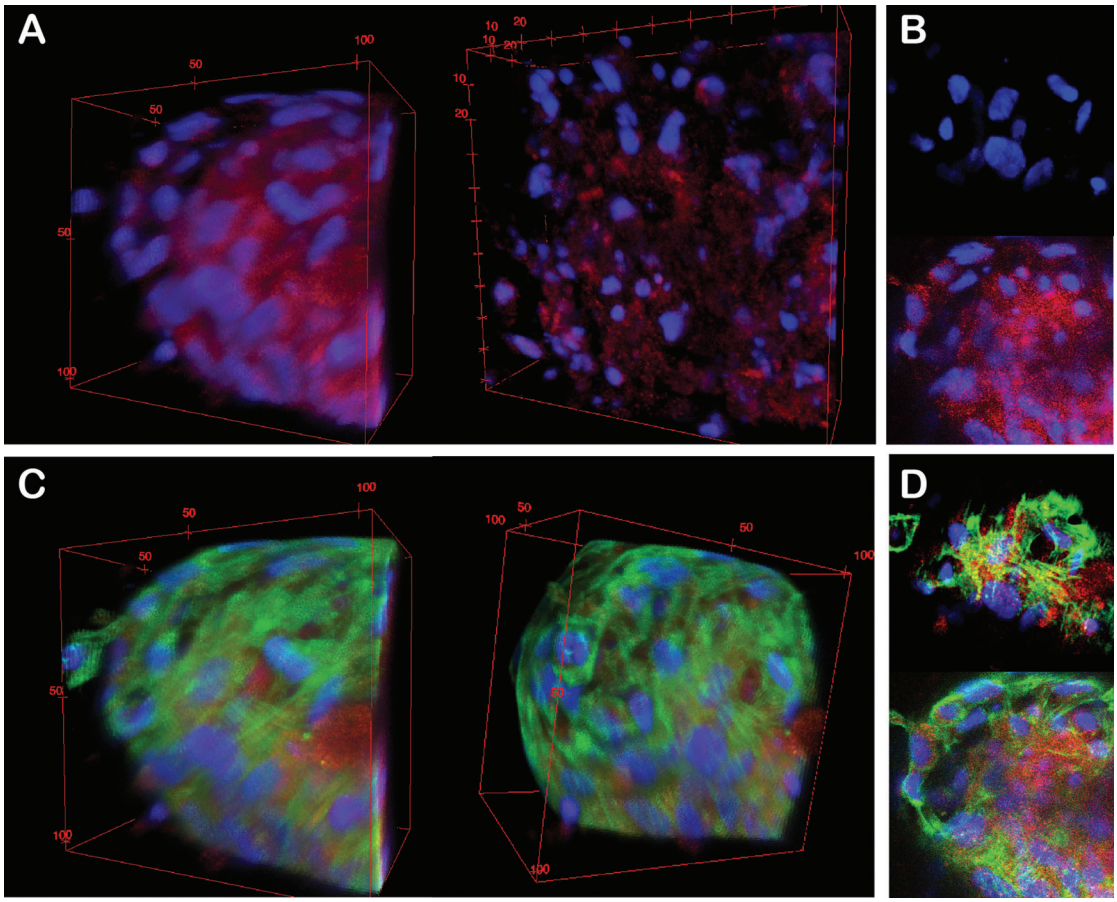

Figure 6. 3D reconstruction of spheroids incorporated in the hydrogel after bioprinting and post-chondrogenic differentiation for 28 days. A) Intense expression of collagen II (red) involving the cells (blue). B) The cell nuclei presented a more ellipsoid than circular pattern and collagen II seems to be maintained in the innermost region of the spheroid. C) F-actin (green) filaments were also highly expressed, and filaments seem to be wrapping the cells and interacting with collagen II. D) F-actin was more detected in the outermost region of the chondrogenic spheroids. Scale bars are presented using red dotted lines considering the 3D projection (axis *x*, *y*, and *z*).

process (Figure 5F). Moreover, the GAG deposition increased over time when analyzed in the final week of chondrogenic differentiation (days 24, 27, and 28) (Figure 5G), while no increase was observed in basic conditions. On the last day of differentiation (day 28), 20.01 ± 1.10 μg mL^{-1} of GAG was quantified in chondrogenic spheroids, in contrast of 4.75 ± 0.90 μg mL^{-1} for the basic spheroids (90 spheroids in each condition, in triplicate). Hence, analyzing GAG production, quantification and expansion of chondrogenic spheroids that occurred during the chondrogenic differentiation period of 28 days, the potential of the differentiation post-bioprinting approach was confirmed.

The presence of collagen II detected by immunostaining was clearly demonstrated in the whole structure of the spheroids in the bioprinted constructs (Figure 5E). Since polysaccharide hydrogels can be non-specifically stained, control filaments printed only with hydrogels were analyzed, as well as autofluorescence of each secondary antibodies and all of them showed negative signals when stained for collagens types I, II, F-actin, and nuclei (Figure S12, Supporting Information).

To further corroborate our findings, constructs under chondrogenic differentiation were sliced to investigate the presence of collagen types I, II, IV, and X at day 1 (constructs 24 h after bioprinting) and day 28 (after chondrogenic differentiation) (Figure 5H). Collagen I was present on days 1 and 28, in contrast to collagen II, which was detected only on day 28, as previously confirmed. The presence of collagen I in the initial structure of the hMSC spheroids at day 1, in contrast to collagen II was also investigated. For that, the relative expression using qPCR analysis of hMSC spheroids and single hMSC cells in suspension was quantified. The relative expression of collagen I was detected in both and significant differences were not observed between spheroids and single cells (Figure S13, Supporting Information). In contrast, the relative expression of collagen II could not be detected in either single cells or spheroids. It can be concluded that collagen I was always present in the bioprinted constructs, while collagen II was produced over 28 days due to the efficient differentiation process. Collagen IV was scarcely present on day 1, but was extensively detected on day 28, and collagen X that was present on both day 1 and 28 (Figure 5H).

Aiming to understand how the cells were embedded in the collagen II network after the differentiation process over 28 days, a confocal microscopy analysis followed by a 3D reconstruction of the spheroids was performed (**Figure 6**). Intense expression of collagen II was observed associated with cells and F-actin

© 2023 The Authors. Advanced Healthcare Materials published by Wiley-VCH GmbH

21922659, 2023, 19, Downloaded from https://advanced.onlinelibrary.wiley.com/doi/10.1002/adhm.202203021 by Spanish Cochrane National Provision (Ministerio de Sanidad), Wiley Online Library on [26/01/2026]. See the Terms and Conditions (https://onlinelibrary.wiley.com/terms-and-conditions) on Wiley Online Library for rules of use; OA articles are governed by the applicable Creative Commons License

throughout the whole 3D structure of the spheroids. Cell nuclei presented a more ellipsoid (sphericity ranging from 0.70 to 0.91 μm, in average 0.083 ± 0.06) than circular (sphericity >0.9) pattern (Figures 6A-B) and collagen II seems to be maintained in the most inner region of the spheroid (Figures 6B,D), in contrast to F-actin that seems to involve the structure in the outermost region (Figures 6C,D).

Last, one of the big challenges of tissue engineering is to maintain the stability of the constructs during long periods of the maturation process with satisfactory cell viability. As abovementioned, cell viability in basic culture medium was satisfactory for 28 days, but an improvement in metabolic activity was noticed when spheroids were cultured in chondrogenic media for the same period. To investigate if this trend could be observed for longer periods, the culture time was extended up to 56 days (twice the initial time). As expected, the same behavior was observed. Bioprinted spheroids cultured in chondrogenic medium for 56 days showed higher metabolic activity when compared with those cultured in basic medium (Figure S15A, Supporting Information).

Corroborating with what was observed at day 28 (Figure 5), profuse ECM production, along with spheroid expansion toward the hydrogel was observed in encapsulated spheroids cultured in chondrogenic media for 56 days (Figure S15B, Supporting Information). High levels s of collagen types I, II, F-actin (Figure S15C, Supporting Information) and GAG were demonstrated in the material secreted by cells in the $XG_{3.75}$:$A_{1.12}$ hydrogel cultured with chondrogenic media at days 28 and 56. The analysis was also performed in the spheroid microwell system, in the absence of the $XG_{3.75}$:$A_{1.12}$ hydrogel, as a control. Abundant ECM production was also observed over 56 days in this system (Figure S16, Supporting Information).

3. Discussion

Mature cartilage tissue has limited regenerative capacity upon damage or disease.[2] Multiple tissue engineered approaches have been investigated over the last decades but with limited translation to patients.[69] The use of injectable hydrogels has been showing significant progress in terms of minimizing manipulation and performing implantation in a short periods.[45] However, lack of mechanical strength and physiological stability have hampered their use as potential implants in large lesions.[46] Instead of using manually injectable hydrogels, herein we established a robust and reproducible bioprinting method to generate stem cell spheroid-loaded bioinks. After bioprinting, these stable constructs were further differentiated in a post-printing step and presented good secretion of relevant ECM molecules and chondrogenic tissue maturation.

Generally, bioprinted approaches to achieve cartilaginous tissue investigate the pre-differentiation of spheroids toward cartilage that are subsequently combined into a 3D construct with or without a hydrogel either by bioprinting or molding.[38,40–43,47,48] Despite the success of using these chondrogenic induced spheroids, fusion capacity and remodeling may be impaired after new tissue formation, preventing overall new tissue fusion in a macro scale.[43]

On the other hand, excessive contact between spheroids can also lead to intense fusion which generally results in a big cell mass, resulting in a hypoxic aggregate with a necrotic core without organization.[23] Thus, instead of using chondrogenic induced spheroids, hMSC not differentiated spheroids formed during 5 days showed to be the ideal timepoint when compared to 7-day spheroids and these were bioprinted in combination with a polysaccharide-based hydrogel using XG and A. The hMSC 5-day spheroids ensured sufficient metabolic activity, also showing easier remodeling during encapsulation due to the reduced amount of newly secreted ECM.

Several hydrogel formulations using XG and A were investigated and an improvement of the bioprinting process was observed depending on the ratio of the polysaccharides investigated. Constructs with a hydrogel composed solely of XG showed low stability after bioprinting due to limited biocompatible crosslinking strategies. Crosslinking of XG chains using trivalent iron ions was previously demonstrated through a reversible sol-gel process.[49] However, cell cytotoxicity effects were not yet investigated for this alternative. The addition of alginate to XG-hydrogels allowed easy and safe crosslinking of the final structure even for bioinks containing cell spheroids.

The $XG_{3.75}$:$A_{1.12}$ hydrogel ensured impressive long-term stability in culture medium (up to 56 days), while sustaining viability of encapsulated spheroids which produced profuse ECM. This is a strength of this hydrogel system that can also lead to a drawback since iis hard to be fully degraded or removed for further analysis. As already reported, swelling of XG can be intense when embedded in distilled water (≈1000% in 4 h) at room temperature and even higher at 37 °C (1400%).[50] Interestingly, besides the progressive increase in swelling over 28 days in culture medium, a slow swelling kinetics was observed when combining XG and A. Even though the ionic strength of culture medium plays a relevant role, the increasing concentration of A in the XG-formulations allows for more crosslinks to be formed, improving the network density and modulus. Herein, the swelling kinetics could be modulated, leading to only 147% after 28 days in culture, while allowing for a profuse ECM production. As previously reported, damage in collagen fibers of the secreted ECM might be an undesirable effect of intense swelling of hydrogels.[51] Thus, the $XG_{3.75}$:$A_{1.12}$ hydrogel formulation is ideal for chondrogenic long-term culture.

As expected, the stiffness of the $XG_{3.75}$:$A_{1.12}$ hydrogel was much lower than that reported for native articular cartilage, which generally can range from 200 to 500 kPa (G′ values), depending on the region and tissue depth.[52,53] However, fully developed native cartilage tissue is not the most reliable model to be used as a reference for cartilage tissue engineering, since tissue constructs are composed of comparatively smaller amounts of newly formed ECM.[52] Moreover, the maturation process of cartilage tissue involves mechanical stimuli, and its adult structural form is achieved during the second decade of life for humans,[25] which is far from what could have been investigate in vitro herein. A more reliable model to compare is immature cartilage, for example, fetal and newborn tissues, since the levels of maturation and organization are not fully established. A previous study reported that in the top cartilage region, fetal and newborn bovine cartilages showed values of 28 ± 13 and 141 ± 10 kPa, respectively, which increased by a factor of 4–5 in the deeper layers.[52] As herein presented, the shear modulus of the XG:A crosslinked hydrogels ranged from 0.6 to 2.2 kPa as the proportion of alginate

© 2023 The Authors. Advanced Healthcare Materials published by Wiley-VCH GmbH

21922659, 2023, 19, Downloaded from https://advanced.onlinelibrary.wiley.com/doi/10.1002/adhm.202203021 by Spanish Cochrane National Provision (Ministerio de Sanidad), Wiley Online Library on [26/01/2026]. See the Terms and Conditions (https://onlinelibrary.wiley.com/terms-and-conditions) on Wiley Online Library for rules of use; OA articles are governed by the applicable Creative Commons License

21922659, 2023, 19, Downloaded from https://advanced.onlinelibrary.wiley.com/doi/10.1002/adhm.202203021 by Spanish Cochrane National Provision (Ministerio de Sanidad), Wiley Online Library on [26/01/2026]. See the Terms and Conditions (https://onlinelibrary.wiley.com/terms-and-conditions) on Wiley Online Library for rules of use; OA articles are governed by the applicable Creative Commons License

increased from 0.75% to 1.5% (*w*/*v*). These values refer to $XG_{3.75}$:$A_{1.12}$ hydrogel without cell spheroids, thus in a long-term maturation is expected that the spheroid density will potentially influence the final mechanical properties of the constructs.

Despite the final aim being to achieve stable cartilaginous tissue constructs with properties in the range of mature cartilage, a fine balance between the optimal mechanical properties and those suitable for chondrogenic differentiation and maturation is still not fully understood. It has been reported that chondrogenic differentiation was more pronounced in soft gelatin-based hydrogels (5% and 7.5% of polymer concentration corresponding to hydrogel stiffness of 538 ± 91 and 3584 ± 146 Pa, respectively) compared with a stiffer formulation (10% solution, enhancing stiffness to 7263 ± 287 Pa). This could have happened due to the easier cell migration and ECM production within the softer hydrogel network.[54] Other studies corroborate with the better chondrogenic phenotype observed in softer hydrogels, such as agarose modified with Arg-Gly-Asp (RGD) and Arg-Gly-Glu (RGE) adhesion sequences[55] and poly(ethylene glycol).[56] The ideal balance should be found between hydrogel stiffness and mesh size, thus aiming to meet processability conditions for bioprinting as well as to facilitate the diffusion of growth factors, and finally, to mainthe chondrogenically differentiated cells and newly secreted ECM.

Using extrusion-based bioprinting with spheroid-loaded bioinks, stable and highly viable bioprinted constructs were obtained, with overall construct thicknesses from 2 to 2.4 mm, within the range expected of human articular cartilage (≈2 to 4 mm).[57] As demonstrated in our work, the approach selected to raise cell concentration in the construct was to increase the number of spheroids, instead of their size, which can cause undesirable results such as apoptosis due to higher shear stress during extrusion. Therefore, pattern fidelity and resolution would be maintained within the oxygen diffusion limit depth in spheroids (up to 200 µm),[58] thus favoring spheroid fusion and larger tissue formation.[38] Autologous chondrocyte implants used in clinical treatments range from 0.5 to 14×10^6 cells cm^{-2}.[59] The licensed approach Chondrosphere (co.don, Teltow, Germany) uses a range between $2–14 \times 10^6$ cells cm^2 organized in chondrocyte spheroids of 500–800 µm of diameter.[59] De Moor et al.[38] used a cell seeding ratio of 1250 chondrogenic spheroids cm^2 (315 cells per spheroid) in a bioprinting process, resulting in 0.4 million cells cm^2, but the authors suggested an increase to 6340 spheroids cm^2 to reach about 2 million cells cm^2. Here, as a proof of concept to achieve a value that agrees with the clinical range, biological constructs with thickness of ≈4 mm were fabricated containing up to 200 spheroids, resulting in 0.6 million cells cm^2. The use of high cell densities in suspension was already demonstrated through bioprinting, such as implemented in an ear cartilage reconstruction[60] and in a lung-mimicking structure[61] reaching $4–5 \times 10^7$ cells mL^{-1} of hydrogel. Overall, the relation behind how the seeding density influences cartilage repair remains under investigation.

The use of spheroids is an efficient approach for large-scale manufacturing of human tissues, allowing bioprinting using a big amount of cells, with high level of control and automation.[48] However, due to the high number of spheroids used in the present study, these tended to be more concentrated on the external borders, where higher hydrogel deposition generally occurs and open pores could not be effectively maintained due to the flow behavior of the bioink. Future improvements on spheroid printing density would require technological development to allow an appropriate dispensing while preventing high shear stresses or nozzle occlusion. Nevertheless, it should also be noted that cell distribution is not homogeneous in all tissues and organs. In fact, articular cartilage is one of the best examples of cell distribution heterogeneity in the human body.[25] Thus, the heterogeneous dispersion of spheroids within the constructs may be an attractive strategy for bioprinting gradients to better mimic the inherent heterogeneity of those tissues.

Our results showed a clear evidence of the presence of primary cartilage-specific proteins, GAGs and collagen II, as a proof of in vitro chondrogenic hMSC differentiation.[67] Moreover, the combination of hMSC aggregates with hydrogels has been presented as a simple but powerful strategy to stimulate abundant cartilage ECM formation when compared to the single cells approach.[62] ECM was extensively secreted to the surrounding $XG_{3.75}$:$A_{1.12}$ hydrogel microenvironment both at day 28 and at day 56, with high levels of released GAG (20.01 ± 1.1 µg mL^{-1}) at day 28. Our findings are in accordance with the results of De Moor et al.,[38] which also demonstrate the successful production of bioprinted constructs with chondrogenic phenotype and satisfactory cell viability. However, the authors induced chondrogenesis for 14-day period before encapsulating these cartilagenous spheroids within a photocrosslinked gelatin-methacrylamide hydrogel via extrusion-based bioprinting. In contrast, in our work, bioprinting was performed using hMSC spheroids and the chondrogenesis was induced in a viscous and natural-based hydrogel in a post-bioprinting process. This finding has a great significance, since it is robust, flexible and not limited to cartilage tissue engineering. Many other lineages can be further investigated using this approach, i.e., osteogenic, neural, and adipogenic lineages.

The expression of collagens I, IV and X obtained in the present study is consistent with previous studies in which pre-differentiation was used.[38,43,47] Collagen I is present on the surface region of articular cartilage and the ratio between col II and col I is frequently used as an indicator of the chondrocyte differentiation state.[25] Agreeing with data previously reported,[38,64] in our work collagen I was always detected, both in 5-day spheroids and the bioprinted constructs, from days 1 to 28, when hMSC differentiation was performed in the hydrogel. An inverse relationship was observed for collagen II, which was not present in the beginning, but was highly expressed at day 28. Collagen X is frequently reported in the literature as a marker of hypertrophic chondrocytes and generally increases during chondrogenesis within time.[67] As demonstrated by Xu et al.,[64] collagen X was not expressed at day 0 during hMSC chondrogenic differentiation in 3D alginate hydrogels. It was significantly increased within 12 and 18 days of culture, reaching a notable 165-fold expression at day 24. Solchaga et al.[65] also reported the detection of type II and X collagen at day 14 throughout cell aggregates under chondrogenic differentiation. Herein, collagen X was identified at day 1 after bioprinting and on day 28, with no detectable differences between them. Thus, it suggests that collagen X was not produced during the differentiation period, or it was produced in a much inferior amount compared to Xu et al.[64] work. This difference can be related to the combination of conditions investigated in the present study. The hydrogel is mainly

© 2023 The Authors. Advanced Healthcare Materials published by Wiley-VCH GmbH

21922659, 2023, 19, Downloaded from https://advanced.onlinelibrary.wiley.com/doi/10.1002/adhm.202203021 by Spanish Cochrane National Provision (Ministerio de Sanidad), Wiley Online Library on [26/01/2026]. See the Terms and Conditions (https://onlinelibrary.wiley.com/terms-and-conditions) on Wiley Online Library for rules of use; OA articles are governed by the applicable Creative Commons License

composed of XG, which has the capability to protect the articular cartilage, reducing damage and further differentiation into a hypertrophic phenotype.[34,35] In addition, the use of TGF-ß1 can inhibit growth plate chondrocyte hypertrophy, along with dexamethasone, which delays the appearance of type X collagen.[67] Probably, this combination of conditions was beneficial to avoid that the levels of collagen X would substantially increase as often observed. Collagen type IV is one of the major protein components of the basement membrane structure, along with laminin, and it is known to bind with proteoglycans. Collagen type IV was not identified on day 1, but identified at day 28, and may be a result of new interconnections among the ECM molecules.[66]

4. Conclusion

Polysaccharide-based hydrogels were combined with stem cell spheroids to obtain stable bioinks and bioprinted constructs for long-term post-bioprinting differentiation. Our work provides immunohistochemical, histological, cellular and molecular evidence corroborating that in vitro chondrogenic differentiation of hMSC spheroids in a post-bioprinting step is a feasible approach. The bioprinted constructs were viable for up to 56 days and showed abundant ECM production, with enhanced collagen type II and type IV secretion up to 28 days. The chondrogenic constructs presented in this research can, in the short-term, be used as 3D model studies for different cartilage diseases, like osteoarthritis. In the long-term, they can be potentially validated as chondral implants aiming to reduce manipulation, allowing the fast generation of patient-specific implants while avoiding the need for lengthy pre-differentiation of spheroids. We envision that a pre-commitment of hMSCs could be shortened and the differentiation post implantation in situ could occur in a faster time, increasing its scalability. Based on this in vitro proof-of-concept, the presented approach holds promise in the future, but still requires further in vivo validation.

5. Experimental Section

Preparation of Xanthan Gum-Alginate Formulations and Vial Inversion Test for Preliminary Screening Viscous Behavior: Xanthan gum (XG) from *Xanthomonas campestris* (G1253, lot #SLCC2817, Sigma-Aldrich), medium viscosity sodium alginate (A) from *brown algae* (W201502, lot #MKBV7858V, Sigma-Aldrich) and DPBS (modified Dulbecco's phosphate-buffered saline, without calcium chloride and magnesium chloride, D8537, Sigma-Aldrich) were used for hydrogel preparation. Nine formulations of XG:A hydrogels were produced varying both mass content (%) and XG:A mass ratio, as described in Table S1, Supporting Information. For the preparation of XG stock solutions, the mass of the polysaccharide in powder form sufficient to prepare a 5% (*w/v*) stock solution was sterilized by fast autoclaving (pre-vacuum sterilizer, 134 °C, 4 min cycle). After cooling to about 20 °C, it was mixed with sterile DPBS and maintained in a roller tube platform overnight to ensure complete dissolution of the polysaccharide. In the case of alginate, the polysaccharide was dissolved in DPBS at a concentration of 4.5% (*w/v*) under magnetic stirring for 1 h, at room temperature. This solution was then sterilized by filtering through a 0.22 µm polyethersulfone (PES) membrane (Sigma-Aldrich).

The stability of these formulations was analyzed by flask inversion, in which the hydrogels were induced to flow by gravity. The flow behavior of each hydrogel was assessed by a time-lapse sequence of pictures after 1 min, 5 min, and 24 h.

Rheological Characterization of the Hydrogels: The rheological characterizations were performed with the formulations that did not flow in the vial inversion test. Rheological analyses were performed on a TA instrument DHR-2 Rheometer equipped with a Peltier temperature controller. The measurements were performed with crosslinked and non-crosslinked hydrogels at 20 °C. Crosslinked hydrogels were produced using hydrogel precursor solutions after exposed to calcium chloride ($CaCl_2$) solution (125 mM) for 10 min. The hydrogels were stored in culture medium at room temperature prior to the analysis. Non-crosslinked hydrogel precursor solutions were loaded into a 20 mm cone-plate geometry holder and oscillatory time sweeps were performed at 1% strain and 0.5 Hz for 300 s to assess the shear modulus of the different formulations. Oscillatory frequency sweeps were taken from 100 to 0.1 rad s^{-1} with a strain of 1%, while flow sweeps (continuous rotation) were acquired with shear rates of 1×10^{-4} s^{-1} to 1000 s^{-1}, with the scaled time average set to 1 (equilibration and measurement time scales inversely proportional to the shear rate). Immediately following the flow sweep, the time sweep measurement was repeated to assess the recovery of the precursor solution post-shear. Finally, oscillatory strain amplitude sweeps were acquired at 0.5 Hz from 0.1% to 100% strain. All measurements were performed in at least triplicate.

Analysis of Extruded Filaments of the Hydrogel Formulations: A pressure-assisted extrusion bioprinting technique (BioScaffolder 3.1, Gesim – Gesellschaft für Silizium-Mikrosysteme mbH, Germany) was used to manufacture all constructs. The hydrogel solutions were loaded into clear syringe barrels (7012074, Nordson) at room temperature, centrifuged at 1000 rcf for 3 min, and coupled to the cartridge holder. The nozzle chosen had a conical geometry and a tapered tip with an internal diameter of 250 µm (7018391, Nordson). Prior to use, syringes and nozzles were disinfected by soaking in ethanol solution (70% v/v) overnight and fully dried. To evaluate the attachment of the hydrogel filaments to the surface, filament formation was analyzed in dry and wet conditions. For the dry condition analysis, the filament was printed directly on a non-treated polystyrene (PS) well plate and for the wet condition, on the PS well plate containing $CaCl_2$ crosslinking agent (1 mL, 125 mM, 10 min). The cartridge and environment temperatures were not controlled, but room temperature was maintained at ≈20 °C. The dry approach was chosen to continue the optimization.

Printability of formulations that passed the vial inversion test was analyzed by printing four-layered scaffolds at speed of 60 mm s^{-1} and pressure of 50 kPa by sequential layer deposition following a square model (1 × 1 cm) composed of a meander with 750 µm interfilament spacing. Three independent constructs were evaluated for each hydrogel formulation. Further studies were performed with a formulation containing the highest amount of alginate aiming at ensuring the formation of a minimum amount of visible macropores.

Analysis of Extruded Filaments of $Xg_{3.75}$:$A_{1.12}$ Formulation as a Function of Speed, Pressure, and Nozzle Diameter: Filament formation of $XG_{3.75}$:$A_{1.12}$ hydrogel in different printing conditions was analyzed using a 250 µm internal diameter nozzle. One-layer scaffolds were printed in triplicate. The scaffolds were ionically crosslinked by soaking in $CaCl_2$ solution (125 mM, 10 min) and afterward, washed using PBS. An exploratory study was conducted varying printing speed from 30 to 70 mm s^{-1} and printing pressure from 30 to 80 kPa. Based on this step, a parametric investigation was performed in more detailed ranges. For this, the speed was kept at 40 mm s^{-1} and the pressure was varied at 50, 60, or 70 kPa. Afterward, pressure was maintained at 70 kPa and speed values of 50 or 60 were applied. To compare filaments obtained over different speed and pressure values, optical microscopy pictures (Nikon Eclipse TS 100) were taken immediately after printing (day 0).

To evaluate if the nozzle gauge could control the filament diameter, another conical tapered nozzle with 410 µm internal diameter (7018298, Nordson) was analyzed and compared with the 250 µm nozzle. The dimensions of 10 filaments of three scaffolds printed with each nozzle were quantified using Image J. The coalescence effect was also analyzed by comparing the diameter of the printed filaments with the internal diameters of the nozzles.

After the optimization for the best printing parameters, scaffold geometric features, filament diameter, pore size (in X and Y axes) and total scaffold porosity of four independently printed scaffolds were analyzed using Image J and compared to the preset CAD model.

© 2023 The Authors. Advanced Healthcare Materials published by Wiley-VCH GmbH

Scaffold Shape Stability Analysis in Culture Medium Over 50 Days: Scaffold stability was analyzed for long period exposure in basic culture medium. The 1 × 1 cm scaffolds previously printed in triplicate (2.4 section) were ionically crosslinked by soaking with $CaCl_2$ solution (125 mM, 10 min), and maintained in culture media in the incubator for 50 days. To analyze if the printed shape was maintained and if degradation occurred with time, optical microscopy pictures were taken at day 10, 20, 30, and 50, and compared to those of scaffolds obtained immediately after printing (day 0).

Swelling Index and Mass Change of Printed Scaffolds in Basic Culture Medium: To evaluate the swelling and mass changes of the $XG_{3.75}$:$A_{1.12}$ hydrogels in culture medium, fifteen four-layer-scaffolds were printed, ionically crosslinked with $CaCl_2$ (125 mM, 10 min) and washed with PBS. Immediately after that, the masses of three freshly prepared printed scaffolds (W_0, initial mass) were determined in a high precision scale, and then the specimens were frozen at −20 °C. The remaining twelve scaffolds were immersed in 1 mL each of basic culture medium in a 12-well plate and kept in the incubator. The culture medium of each well was partially changed every 72 h by replacing half of the medium with fresh medium. On days 7, 14, 21, and 28, three scaffolds were collected, the excess of culture medium was removed by blotting, their masses were determined (W_t, final mass), and then the specimens were frozen at −20 °C. The swelling ratio was calculated as described by Sarker et al.,[44] using Equation 1:

$$\text{Swelling ratio} = \left(\frac{(W_t - W_0)}{W_0} \right) \times 100 \quad (1)$$

All frozen scaffolds were lyophilized and analyzed regarding their final masses. To determine the mass change over time, Equation 2 was used, in which M_0 is the mass of scaffolds lyophilized immediately after fabrication and M_f is the mass of the lyophilized materials at each time point:

$$\text{Mass change} = \left(\frac{\left(M_f - M_0\right)}{M_0} \right) \times 100 \quad (2)$$

To analyze the crosslinking effect on hydrogel stability, two hydrogels formulations ($XG_{3.75}$:$A_{1.12}$ and $XG_{5.00}$:$A_{0.00}$) were kept in culture medium. The $XG_{5.00}$:$A_{0.00}$ (alginate-free formulation) was also tested in the presence or absence of the $CaCl_2$ crosslinking agent (125 mM, 10 min) to investigate its eventual effect on XG. Samples were analyzed for up to 45 days.

Cell Culture Conditions and Spheroid Formation: The culture media used in this work will be referred to as basic and chondrogenic media. The basic medium was composed by MEM Alpha Medium with GlutaMAX (32561-029, Gibco), supplemented with 10% (v/v) of fetal bovine serum (FBS, F7524, Sigma-Aldrich) and 1% penicillin/streptomycin solution (Pen-Strep, 11 548 876, Thermo Fisher). The chondrogenic medium was based on the composition defined by Johnstone et al.[67] and freshly prepared every week. It was composed of 4.5 g L^{-1} high-glucose DMEM medium (31966-021, Gibco), supplemented with 50 mg mL^{-1} of Insulin-Transferrin-Selenium (ITS premix, 41400-045, Gibco, USA), 40 mg mL^{-1} of proline (P5607, Sigma-Aldrich), 57.8 µg mL^{-1} of ascorbic acid (A8960, Sigma-Aldrich), 0.1 µM of dexamethasone (D8893, Sigma-Aldrich), 10 ng mL^{-1} of TGF-ß1 (100-21, PeproTech) and 1% (v/v) of Penstrep.

Suspensions of human mesenchymal stromal cells (hMSC) containing 2 × 10^6 cells in passage 2 (8F3543, Lonza) were used to prepare the working cell stock. The cells were expanded in basic culture medium by culturing 3000 cells cm^2 on T-175-cm^2 flasks until they reached 70% of confluence up to passage 3. The cell stock was divided into cryovials and stored in liquid nitrogen until further use. For each experiment, a fresh vial containing 5 × 10^5 cells was thawed and expanded in the same conditions until passage 6 to prepare cell suspensions to produce hMSC spheroids.

The microwell array insert used to produce hMSC spheroids was previously described in detail.[63] Briefly, using a cast previously obtained by additive manufacturing, several array inserts were obtained through micromolding, using a non-adhesive hydrogel made of sterile ultrapure 3% (*w/v*) agarose (16 500 100, Invitrogen) in PBS solution. The microwell array inserts were manufactured the day before cell seeding, immersed in basic culture medium and maintained in the incubator overnight. A total of 5 × 10^5 cells were seeded in each microwell array consisting of 164 cavities, resulting in spheroids containing an average of 3048 cells. The spheroids were cultured until day 5 or 7 and the culture medium was refreshed every 48 h.

All cell culture experiments were performed at 37 °C, pH 7.2 under a 5% CO_2 atmosphere.

Biochemical Assays: To analyze the viability of the cells in the spheroids and printed constructs, a live/dead assay was carried out with a staining solution consisting of 2.5 µM of ethidium homodimer-1 (EthD-1, E1169, Thermo Fisher) and 1 µM of calcein acetoxymethyl (Calcein AM, c3099, Thermo Fisher). The samples were analyzed with a fluorescence microscope (Eclipse Ti-E Nikon, Japan).

The Cell Titer-Glo 3D assay (G9682, Promega, USA) was used to quantify metabolic activity. This assay measures ATP in 3D microtissues as an indicator of viability by means of a luminescent readout. Equal volumes of reagent and culture medium were added to 5 and 7-day spheroids. After shaking for 30 min at 30 rpm, at room temperature, luminescence was determined (integration time of 0.25–1 s per well) using the CLARIOstar plate reader (BMG Labtech). Two control groups (dead spheroids representing non-metabolically active cells and single hMSC cells in suspension) were used as references of the luminescent readout. The procedure described above was equally performed for both control groups, but in the first one, a previous treatment using directly dimethyl sulfoxide (DMSO) solution for 2 h was performed to kill the cells (procedure adapted from Amaral et al.[68]). On the second control, single cells were used to verify metabolic activity prior to spheroid formation. The corresponding numbers of cells in suspension were used instead of spheroids (≈3048, 15243, 45731, and 91463 cells, equivalent to 1, 5, 15, and 30 spheroids, respectively). This experiment was repeated three times, using three different array inserts.

An adapted protocol was used to analyze cell metabolic activity of spheroids in the hydrogel constructs. Only constructs having the same or presenting a narrow range of spheroids were analyzed together (the number of spheroids is described in the specific figures' caption). Scaffolds without spheroids were printed to be used as negative controls and to exclude any potential interference cause by the hydrogels. All assays were performed in triplicate.

The sulfated glycosaminoglycan (sGAG) content was quantified using 1,9-dimethylmethylene blue (DMMB) dye. Spheroids and supernatant were collected at each medium refreshment during the last week of chondrogenic differentiation and used to quantify the total amount of sGAGs produced and released into the medium. Samples were digested with proteinase K (P6556, Sigma-Aldrich) Tris/EDTA buffer overnight in the thermocycler at 56 °C, 300 rpm. Chondroitin sulfate from shark cartilage was used to prepare the standard curve in the same buffer as the samples. An amount of 25 µL of standard or sample was added to each well of a microplate. An additional 5 µL of NaCl solution and 150 µL of DMMB solution (4 mg DMMB overnight dissolved in 1.25 mL EtOH added to 225 mL dH_2O with 593 mg NaCl and 760 mg glycine; pH = 3) was added to each well and absorbance was measured at 525 and 595 nm.

Bioink Preparation and Bioprinting of Spheroid-Based Constructs: Aiming to analyze different mixing approaches to prepare the bioink, the impact of the pipetting conditions on cell viability was investigated through a live/dead assay. Spheroids were collected, incubated in the live/dead staining solution and transferred to a Petri dish using a 1 mL pipette tip to simulate low stress mixing conditions. To simulate high shear-stress conditions, the spheroids were stained, washed twice and exposed to a vigorous pipetting step (several up-and-down movements) using a 1 mL pipette and only then were transferred to a Petri dish. Both groups were analyzed right after transference with a fluorescence microscope (Eclipse Ti-E Nikon, Japan).

The bioink was prepared by mixing 2500 hMSCs spheroids to 1 mL of $XG_{3.75}$:$A_{1.12}$ hydrogel. Since each spheroid had, in average, ≈3048 cells, a total cell suspension of 7.6 × 10^6 cells mL^{-1} was used. Two different

© 2023 The Authors. Advanced Healthcare Materials published by Wiley-VCH GmbH

21922659, 2023, 19, Downloaded from https://advanced.onlinelibrary.wiley.com/doi/10.1002/adhm.202203021 by Spanish Cochrane National Provision (Ministerio de Sanidad), Wiley Online Library on [26/01/2026]. See the Terms and Conditions (https://onlinelibrary.wiley.com/terms-and-conditions) on Wiley Online Library for rules of use; OA articles are governed by the applicable Creative Commons License

21922659, 2023, 19, Downloaded from https://advanced.onlinelibrary.wiley.com/doi/10.1002/adhm.202203021 by Spanish Cochrane National Provision (Ministerio de Sanidad), Wiley Online Library on [26/01/2026]. See the Terms and Conditions (https://onlinelibrary.wiley.com/terms-and-conditions) on Wiley Online Library for rules of use; OA articles are governed by the applicable Creative Commons License

mixing approaches were evaluated. On the first approach, the hydrogel was added to the spheroid pellet and through mechanical mixing (up and down movements) using a 1 mL gel-loading pipette. On the second, the spheroids were gently pipetted following a line trajectory, while dispensing constantly the spheroids inside a portion of hydrogel, without forced mixing afterward, aiming to reduce the shear-stress.

The setup and parameters of the bioprinting process using spheroids suspend in the hydrogel were defined based on the parametric investigation previously performed with the hydrogel and are summarized in Table S2, Supporting Information.

Morphological Analysis of Spheroids after Bioprinting in Basic Medium: To evaluate the impact of the bioprinting and spheroid encapsulation inside the polysaccharide-based bioinks, bioprinted constructs were cultured for up to 28 days in basic medium. Images of the constructs were taken using an optical microscope (Eclipse Ti-E Nikon, Japan) at days 1, 7, 14, 21, and 28. The diameters in X and Y-axes were measured manually using Image J. The sphericity and solidity indexes were quantified using the Image J (version 1.53e) particle analyzer function, considering a scale ranging from 0 to 1.

Chondrogenic Differentiation Performed on Bioprinted Constructs: The validation of the hMSCs used in this work to differentiate into chondrocytes was assessed using the chondrogenic differentiation protocol described by Penick et al.[70] Briefly, 5×10^5 hMSCs in suspension were placed in a 15 mL tube containing 1 mL of chondrogenic culture medium. The cells were centrifuged (400 g, 2 min) and maintained in the incubator for 24 h. On the following day, the formed cell pellet was detached from the tube by gentle tapping and the same culturing conditions were maintained during 28 days with media refreshment performed three times a week.

Bioprinted constructs were maintained in basic or chondrogenic culture medium as previously described during 28 and 56 days, with medium replacement three times a week. Furthermore, spheroids were encapsulated into the polysaccharide formulation selected for bioprinting and kept up to 56 days in culture in basic or chondrogenic media to analyze ECM production per week, spheroid expansion toward the hydrogel and to compare the metabolic activity.

Histochemical and Immunohistochemical Analysis: Histochemical analysis was performed to evaluate cell and ECM organization of 5 and 7-day old spheroids. Initially, samples (spheroids and constructs) were fixed with 4% paraformaldehyde (PFA) in PBS solution for 30 min and dehydrated through graded washes of ethanol in water (50, 70, 96 and 100%), washed twice with xylene and finally embedded in liquid paraffin at 56 °C overnight. After that, the spheroids were embedded in fresh paraffin and sections of 5 µm in thickness were treated with hematoxylin-eosin (HE) to stain cell nuclei and cytoplasm, Masson's trichrome (MT) to stain collagen, and alcian blue (AB) to stain glycosaminoglycan (GAG).

Immunohistochemical analysis was performed to determine the distribution and shape of cells and also ECM production, as well as the presence of collagen types I, II, IV, X, and F-actin. The assays were performed in fixed samples containing the whole printed construct, or in 5 µm sections, of spheroids or constructs previously embedded in paraffin and sliced.

Due to the complex composition of the whole printed constructs, some modifications were implemented in the immunostaining procedure to ensure efficient stain penetration throughout the sample. In the permeabilization step, the full printed constructs were exposed overnight to a mixture containing 1% Triton X-100, 0.05% Tween-20, 5% goat serum and 1% BSA diluted in PBS. The sliced samples were exposed to 0.1% Triton X-100 diluted in PBS for 10 min. All samples were washed twice with PBS and the blocking step was performed by exposing the specimens to 1% bovine albumin serum (BSA) solution in PBS for 1 h. The primary antibodies (anti-mouse col I, ab6308; anti-rabbit col II, ab34712; anti-rabbit col IV, ab231957 and anti-mouse col X, ab 49 945, Abcam) were diluted (1/200) in 1% BSA solution in the case of the sliced samples and in a mixture consisting of 1% BSA and 0.05% Tween-20 in PBS for the printed constructs. The incubation with the first antibody was performed overnight at 4 °C for both groups. The samples were washed three times with PBS and incubated with the secondary antibody diluted (1/1000) in the same buffer for 1 h at room temperature. After three washing steps, the samples were incubated with phalloidin diluted (1/100) in PBS for 1 h at room temperature. Finally, samples were incubated with DAPI DNA dye, (4′6-diamidine-2′-phenylindole-dihydrochloride) diluted (1:100) in PBS for 15 min at room temperature. The samples were then analyzed using a fluorescence microscope (Nikon Eclipse TI-E microscope, Japan).

Confocal Microscopy and 3D Reconstruction Analysis: Confocal microscopy data of the spheroids and whole constructs were acquired using a confocal laser scanning microscope (Leica TCS SP8, Germany). The images from the same group of analyses were taken on the same day, in triplicate, using the same settings. 3D reconstruction analysis was done using the image-processing package Fiji software (version 2.1.0), Image J.

Live-Cell Imaging of Spheroid Fusion: Time-lapse microscopy was performed using a Nikon Eclipse TI-E microscope (Japan) with an Okolabs environmental control system (37 °C and 5% of CO2 atmosphere) equipped with a Prime 95B sCMOS camera and Lumencor Spectra X Light source. The time-lapse imaging package of NIS Elements Software (Nikon, Japan) was used to monitor the experiments, together with a motorized high-accuracy image capture system. Spheroids were placed close to each other and the total well volume was filled with media (≈50 µL of hydrogel and spheroids + ≈150 µL of medium). The remaining empty wells of the 96-well plate were filled with PBS to aid in the control of atmosphere humidity, avoiding drying of the hydrogel during the time-lapse data acquisition experiment. Measurements were performed using Image J.

Real-Time PCR Analysis: For PCR analysis, the total RNA from the cells cultured in monolayers and in spheroids for 5 days were extracted. Cells and spheroids were lysed adding 1 mL TRIzol directly, the solution was transferred to Phasemaker tubes (A33248, ThermoFisher) followed by the addition of 0.2 mL of chloroform under vigorous shaking for 15 s and the resulting samples were incubated for 3 min at room temperature. Then, the samples were centrifuged at 12 000 g for 5 min at 4 °C and the aqueous phase was transferred to another tube, when 0.5 mL of isopropanol was added. This solution was then incubated at room temperature for 10 min and afterward centrifuged at 12 000 g for 10 min at 4 °C. Finally, the supernatant was removed, leaving only the RNA pellet, which was washed with 75% ethanol, dried and resuspended on RNase-free water. The RNA concentrations were measured using a BioDrop and the complementary DNA (cDNA) was synthetized using the iScript cDNA synthesis kit (Bio-Rad), following the protocol from the manufacturer. The resulting cDNA was diluted and quantified for the qPCR assay. Three biological replicates and three technical replicates were used for the qPCR analysis regarding each of the previously described experimental conditions. The specific primer sequences of collagen I and II are listed in Table S3, Supporting Information.

Statistical Analysis: Statistical analysis was conducted using Prism software (8.4.3 version, GraphPad). One-way or two-way ANOVA was employed with Tukey's post hoc comparison to evaluate statistical significance. The number of replicates and samples are shown in the figures' captions in each case and the data are expressed as mean ± standard deviation (SD) values or represented using standard deviation bars in the graphs.

Supporting Information

Supporting Information is available from the Wiley Online Library or from the author.

Acknowledgements

The authors would like to acknowledge the support to this research by: the National Council for Scientific and Technological Development (Conselho Nacional de Desenvolvimento Científico e Tecnológico – CNPq, Brazil – Grants # 314 724/2021-4, 307 829/2018-9, 430 860/2018-8, 142 050/2018-0 and 465 656/2014-5); the Coordination for the Improvement of Higher Educational Personnel (Coordenação de Aperfeiçoamento de Pessoal de Nível Superior CAPES, Brazil – Finance codes 001, PrInt 88 887.364849/2019-00 and PrInt 88 887.310405/2018-00); the Fund

 © 2023 The Authors. Advanced Healthcare Materials published by Wiley-VCH GmbH

for Support to Teaching, Research and Extension from the University of Campinas (Fundo de Apoio ao Ensino, à Pesquisa e à Extensão – FAEPEX/UNICAMP, Brazil – Grants # 2921/18, 2324/21), the NWE INTERREG BONE grant (#495) and the European Union's Horizon 2020 framework program, call SC1-BHC-07-2019 – Regenerative medicine: from new insights to new applications, JointPromise – Precision manufacturing of microengineered complex joint implants, under grant agreement 874 837. Project website: http://www.jointpromise.eu/). The authors would also like to thank Dr. David Boaventura Gomes (Maastricht University, The Netherlands) for the support on the confocal microscopy and M.Sc. Enrique Escarda Castro (Maastricht University, The Netherlands) for the discussions regarding the molecular biology assays.

After initial online publication, the reference list and some citations were corrected on May 13, 2023, as some were originally mixed up during processing. The editorial office apologizes for any inconvenience caused.

Conflict of Interest

The authors declare no conflict of interest.

Data Availability Statement

The data that support the findings of this study are available from the corresponding author upon reasonable request.

Keywords

bioprinting, chondrogenic differentiation, hydrogel, mesenchymal stromal cells, spheroids

Received: November 21, 2022
Revised: March 13, 2023
Published online: May 3, 2023

[1] D. J. Hunter, L. March, M. Chew, *Lancet* **2020**, *396*, 1711.
[2] E. B. Hunziker, *Osteoarthritis Cartilage* **2001**, *10*, 432.
[3] D. J. Hunter, S. Bierma-Zeinstra, *Lancet* **2019**, *393*, 1745.
[4] X. Li, Y. Liang, X. Xu, J. Xiong, K. Ouyang, L. Duan, D. Wang, *Biomed Res. Int.* **2019**, *2019*, 1.
[5] H. Holtzer, J. Abbott, J. Lash, S. Holtzer, *Proc. Natl. Acad. Sci. USA* **1960**, *46*, 1533.
[6] P. D. Benya, J. D. Shaffer, *Cell* **1982**, *30*, 215.
[7] A. Nazempour, B. J. van Wie, *Ann. Biomed. Eng.* **2016**, *44*, 1325.
[8] A. Dickhut, K. Pelttari, P. Janicki, W. Wagner, V. Eckstein, M. Egermann, W. Richter, *J. Cell. Physiol.* **2009**, *219*, 219.
[9] S. Y. Song, J. Hong, S. Go, S. Lim, H. S. Sohn, M. Kang, G. J. Jung, J. K. Yoon, M. L. Kang, G. il Im, B-S. Kim, *Adv. Healthcare Mater.* **2020**, *9*, 1901612.
[10] V. Mironov, T. Boland, T. Trusk, G. Forgacs, R. R. Markwald, *Trends Biotechnol.* **2003**, *21*, 157.
[11] K. Jakab, B. Damon, A. Neagu, A. Kachurin, G. Forgacs, *Biorheology* **2006**, *43*, 509.
[12] M. C. Decarli, R. Amaral, D. P. dos Santos, L. B. Tofani, E. Katayama, R. A. Rezende, J. V. L. da Silva, K. Swiech, C. A. T. Suazo, C. Mota, L. Moronzo, A. M. Moraes, *Biofabrication* **2021**, *13*, 032002.
[13] J. Groll, J. A. Burdick, D. W. Cho, B. Derby, M. Gelinsky, S. C. Heilshorn, T. Jüngst, J. Malda, V. A. Mironov, K. Nakayama, A. Ovsianikov, W. Sun, S. Takeuchi, J. J. Yoo, T. B. F. Woodfield, *Biofabrication* **2019**, *11*, 013001.
[14] T. Boland, V. Mironov, A. Gutowska, E. A. Roth, R. R. Markwald, *The Anatomical Record – Part A* **2003**, *272*, 497.
[15] G. Kaushik, J. Leijten, A. Khademhosseini, *Stem Cells* **2017**, *35*, 51.
[16] V. Mironov, R. P. Visconti, V. Kasyanov, G. Forgacs, C. J. Drake, R. R. Markwald, *Biomaterials* **2009**, *30*, 2164.
[17] L. Moroni, T. Boland, J. A. Burdick, C. de Maria, B. Derby, G. Forgacs, J. Groll, Q. Li, J. Malda, V. A. Mironov, C. Mota, M. Nakamura, W. Shu, S. Takeuchi, T. B. F. Woodfield, T. Xu, J. J. Yoo, G. Vozzi, *Trends Biotechnol.* **2018**, *36*, 384.
[18] M. P. Stuart, R. A. M. Matsui, M. F. S. Santos, I. Côrtes, M. S. Azevedo, K. R. Silva, A. Beatrici, P. E. C. Leite, P. Falagan-Lotsch, J. M. Granjeiro, V. Mironov, L. S. Baptista, *Stem Cells Int.* **2017**, *2017*, 7053465.
[19] C. Norotte, F. S. Marga, L. E. Niklason, G. Forgacs, *Biomaterials* **2009**, *30*, 5910.
[20] I. T. Ozbolat, *J. Nanotechnol. Eng. Med.* **2015**, *6*, 024701.
[21] N. Asadi, E. Alizadeh, R. Salehi, B. Khalandi, S. Davaran, A. Akbarzadeh, *Artif. Cells Nanomed. Biotechnol.* **2018**, *46*, 465.
[22] K. Jakab, F. Marga, C. Norotte, K. Murphy, G. Vunjak-Novakovic, G. Forgacs, *Biofabrication* **2010**, *2*, 022001.
[23] S. jeong Kim, H. Byun, S. Lee, E. Kim, G. M. Lee, S. J. Huh, J. Joo, H. Shin, *Acta Biomater.* **2022**, *142*, 60.
[24] C. Mota, S. Camarero-Espinosa, M. B. Baker, P. Wieringa, L. Moroni, *Chem. Rev.* **2020**, *120*, 10547.
[25] S. Camarero-Espinosa, B. Rothen-Rutishauser, E. J. Foster, C. Weder, *Biomater. Sci.* **2016**, *4*, 734.
[26] P. Rastogi, B. Kandasubramanian, *Biofabrication* **2019**, *11*, 042001.
[27] P. Datta, M. Dey, Z. Ataie, D. Unutmaz, I. T. Ozbolat, *NPJ Precis. Oncol.* **2020**, *4*, 18.
[28] Y. Zhao, R. Yao, L. Ouyang, H. Ding, T. Zhang, K. Zhang, S. Cheng, W. Sun, *Biofabrication* **2014**, *6*, 035001.
[29] K. Elkhoury, M. Morsink, L. Sanchez-Gonzalez, C. Kahn, A. Tamayol, E. Arab-Tehrany, *Bioact. Mater.* **2021**, *6*, 3904.
[30] D. Choudhury, H. W. Tun, T. Wang, M. W. Naing, *Trends Biotechnol.* **2018**, *36*, 787.
[31] F. García-Ochoa, V. E. Santos, J. A. Casas, E. Gómez, *Biotechnol. Adv.* **2000**, *18*, 549.
[32] A. F. Dário, L. M. A. Hortêncio, M. R. Sierakowski, J. C. Q. Neto, D. F. S. Petri, *Carbohydr. Polym.* **2011**, *84*, 669.
[33] Z. Liu, P. Yao, *RSC Adv.* **2015**, *5*, 103292.
[34] G. Han, G. Wang, X. Zhu, H. Shao, F. Liu, P. Yang, Y. Ying, F. Wang, P. Ling, *Carbohydr. Polym.* **2012**, *87*, 1837.
[35] H. Shao, G. Han, P. Ling, X. Zhu, F. Wang, L. Zhao, F. Liu, X. Liu, G. Wang, Y. Ying, T. Zhang, *Carbohydr. Polym.* **2013**, *92*, 1850.
[36] D. Dyondi, T. J. Webster, R. Banerjee, *Int J Nanomedicine* **2012**, *8*, 47.
[37] C. B. Westin, M. H. T. Nagahara, M. C. Decarli, D. J. Kelly, Â. M. Moraes, *Eur. Polym. J.* **2020**, *129*, 109637.
[38] L. de Moor, S. Fernandez, C. Vercruysse, L. Tytgat, M. Asadian, N. Geyter, S. Vlierberghe, P. Dubruel, H. Declercq, *Front. Bioeng. Biotechnol.* **2020**, *8*, 00484.
[39] R. Burdis, F. Chariyev-Prinz, D. C. Browe, F. E. Freeman, J. Nulty, E. E. McDonnell, K. F. Eichholz, B. Wang, P. Brama, D. J. Kelly, *Biomaterials* **2022**, *289*, 121750.
[40] L. de Moor, M. Minne, L. Tytgat, C. Vercruysse, P. Dubruel, S. van Vlierberghe, H. Declercq, *Macromol. Biosci.* **2021**, *21*, 2000401.
[41] W. Sun, J. Zhang, Y. Qin, H. Tang, Y. Chen, W. Lin, Y. She, K. Zhang, J. Yin, C. Chen, *Adv. Healthcare Mater.* **2022**, *11*, 2200648.
[42] F. Staubli, M. J. Stoddart, M. D'Este, A. Schwab, *Acta Biomater.* **2022**, *143*, 253.
[43] G. N. Hall, I. Rutten, J. Lammertyn, J. Eberhardt, L. Geris, F. P. Luyten, I. Papantoniou, *Biofabrication* **2021**, *13*, 045025.
[44] Md. Sarker, M. Izadifar, D. Schreyer, X. Chen, *J. Biomater.* **2018**, *29*, 1126.
[45] Y. Tu, N. Chen, C. Li, H. Liu, R. Zhu, S. Chen, Q. Xiao, J. Liu, S. Ramakrishna, L. He, *Acta Biomater.* **2019**, *90*, 1.

© 2023 The Authors. Advanced Healthcare Materials published by Wiley-VCH GmbH

21922659, 2023, 19, Downloaded from https://advanced.onlinelibrary.wiley.com/doi/10.1002/adhm.202203021 by Spanish Cochrane National Provision (Ministerio de Sanidad), Wiley Online Library on [26/01/2026]. See the Terms and Conditions (https://onlinelibrary.wiley.com/terms-and-conditions) on Wiley Online Library for rules of use; OA articles are governed by the applicable Creative Commons License

[46] M. Liu, X. Zeng, C. Ma, H. Yi, Z. Ali, X. Mou, S. Li, Y. Deng, N. He, *Bone Res* **2017**, *5*, 17014.
[47] J. Bolander, C. Mota, H. W. Ooi, H. Agten, M. B. Baker, L. Moroni, F. P. Luyten, *Adv. Funct. Mater.* **2021**, *31*, 2104159.
[48] R. Burdis, D. J. Kelly, *Acta Biomater.* **2021**, *126*, 1.
[49] M. Kang, O. Oderinde, S. Liu, Q. Huang, W. Ma, F. Yao, G. Fu, *Carbohydr. Polym.* **2019**, *203*, 139.
[50] A. G. Andreopoulos, P. A. Tarantili, *J. Biomater. Appl.* **2001**, *16*, 34.
[51] R. J. Nims, A. D. Cigan, M. B. Albro, G. Vunjak-Novakovic, C. T. Hung, G. A. Ateshian, *Tissue Eng. Part C* **2015**, *21*, 747.
[52] T. J. Klein, M. Chaudhry, W. C. Bae, R. L. Sah, *J. Biomech.* **2007**, *40*, 182.
[53] G. Peng, S. M. Mcnary, K. A. Athanasiou, A. H. Reddi, *Tissue Eng. Part A* **2014**, *20*, 3332.
[54] S. Zigon-Branc, M. Markovic, J. van Hoorick, S. van Vlierberghe, P. Dubruel, E. Zerobin, S. Baudis, A. Ovsianikov, *Tissue Eng. Part A* **2019**, *25*, 1369.
[55] E. Schuh, S. Hofmann, K. Stok, H. Notbohm, R. Müller, N. Rotter, *J. Tissue Eng. Regen. Med.* **2012**, *6*, e31.
[56] S. J. Bryant, K. S. Anseth, *J. Biomed Mater. Res.* **2002**, *59*, 63.
[57] A. J. S. Fox, A. Bedi, S. Rodeo, *Orthopaedics* **2009**, *1*, 461.
[58] E. J. Levorson-Wright, M. Santoro, F. K. Kasper, A. G. Mikos, *Compr. Biomat.* **2011**, *5*, 1.
[59] C. B. Foldager, A. H. Gomoll, M. Lind, M. Spector, *Cartilage* **2012**, *3*, 108.
[60] H. W. Kang, S. J. Lee, I. K. Ko, C. Kengla, J. J. Yoo, A. Atala, *Nat. Biotechnol.* **2016**, *34*, 312.
[61] B. Grigoryan, S. J. Paulsen, D. C. Corbett, D. W. Sazer, C. L. Fortin, A. J. Zaita, P. T. Greenfield, N. J. Calafat, J. P. Gounley, A. H. Ta, F. Johansson, A. Randles, J. E. Rosenkrantz, J. D. Louis-Rosenberg, P. A. Galie, K. R. Stevens, J. S. Miller, *Science 1979* **2019**, *364*, 458.
[62] L. S. Moreira Teixeira, J. C. H. Leijten, J. Sobral, R. Jin, A. A. van Apeldoorn, J. Feijen, C. van Blitterswijk, P. J. Dijkstra, M. Karperien, *Eur. Cell Mater.* **2012**, *23*, 387.
[63] M. C. Decarli, M. V. de Castro, J. A. Nogueira, M. H. Nagahara, C. B. Westin, A. L. Oliveira, J. V. L. Silva, L. Moroni, C. Mota, Â. M. Moraes, *Biomater Adv.* **2022**, *135*, 112685.
[64] J. Xu, W. Wang, M. Ludeman, K. Cheng, T. Hayami, J. C. Lotz, S. Kapila, *Tissue Eng. Part A* **2008**, *14*, 667.
[65] L. A. Solchaga, K. J. Penick, J. F. Welter, *Methods Mol. Biol.* **2011**, *698*, 253.
[66] E. Genové, C. Shen, S. Zhang, C. E. Semino, *Biomaterials* **2005**, *26*, 3341.
[67] B. Johnstone, T. M. Hering, A. I. Caplan, V. M. Goldberg, J. U. Yoo, *Exp. Cell Res.* **1998**, *238*, 265.
[68] R. Amaral, M. Zimmermann, A. H. Ma, H. Zhang, K. Swiech, C. X. Pan, *Cancers (Basel)* **2020**, *12*, 1304.
[69] S. Jiang, W. Guo, G. Tian, X. Luo, L. Peng, S. Liu, X. Sui, Q. Guo, X. Li, *Stem Cells Int.* **2020**, *2020*, 5690252.
[70] K. J. Penick, L. A. Solchaga, J. F. Welter, *BioTechniques* **2005**, *39*, 687.

© 2023 The Authors. Advanced Healthcare Materials published by Wiley-VCH GmbH

21922659, 2023, 19, Downloaded from https://advanced.onlinelibrary.wiley.com/doi/10.1002/adhm.202203021 by Spanish Cochrane National Provision (Ministerio de Sanidad), Wiley Online Library on [26/01/2026]. See the Terms and Conditions (https://onlinelibrary.wiley.com/terms-and-conditions) on Wiley Online Library for rules of use; OA articles are governed by the applicable Creative Commons License